CHAPTER III

Structural Characterization of CdSe Thin Films

Chapter III

Structural Characterization of CdSe Thin Films

3.1 Introduction

Different physical properties including the optoelectronic properties /1,2/ of thin films are highly structure sensitive. A thermally deposited thin film may be amorphous, epitaxial or polycrystalline depending upon the factors like nature of substrate /3/, substrate temperature (T_s) /4/, rate /5/ and angle of deposition, order of vacuum, composition of source materials and their vapour pressures etc. Depending upon the methods of preparation and deposition conditions, thin films of II-VI compounds may have ZnS type Zincblende structure or mixed structure. It is seen that structure of a thermally evaporated film mainly depends upon the T_s and the nature of substrate /6/. It is to be noted that the structural characteristics should be properly known for any applications, including thin film based devices. Important structural properties of thin films are crystallinity, unit cell geometry, built-in stress and strain, grain size, lattice faults, dislocation density and foreign imperfections.

Different methods used for the purpose of structural analysis and characterization of the thin films have been reported by many authors /7-12/. At present different sophisticated characterization techniques have emerged and with the help of computer aided analyses, both native and foreign imperfections can be estimated in accurate quantitative form.

The techniques, which are used either for surface characterization or for both surface and volume structural analysis, are based on interactions of radiations and electrons, with the lattice sites occupants of solids. HEED (High energy electron diffraction) and LEED (Low energy electron diffraction) technique are based on the principle of electron diffraction. EM (Electron microscopy), SPM (Scanning probe electron microscopy) /13/ and SEM (Scanning electron microscopy) involve scattering or diffraction and subsequent recombinations of electron waves to form image. FEM, FIM (Field emission or ion microscopy) are based on the principle of emission of X-rays, electrons, ions after the impact of electrons with the material. AES (Auger electron spectroscopy), XPES (X-ray photoelectron spectroscopy), ESCA (Electron spectroscopy

for chemical analysis), LEISS (Low energy ion scattering spectroscopy) and SIMS (Secondary ion mass spectroscopy) have been used for energy and mass analyses for surface layer atoms.

Electron diffraction study is a powerful tool for the observation of lattice defects and other crystallographic features, like structure and surface states of thin films. Transmission electron microscopy (TEM) provides an accurate and comprehensive method for structural analysis /14/ as it processes singletron capability of forming images of lattice defects such as stacking faults, microtwins, dislocations, vacancy clusters and grain domain boundaries with a resolution better than 10Å. But it is a destructive method of analysis because the films have to be detached from its substrate and manipulated on to a supporting grid. The other disadvantage is that the TEM technique cannot be applied to films of thickness greater than 1000Å because such films cannot transmit electrons. The experimental films of the present study bear the thickness greater than 1000Å and were deposited on properly cleaned high quality glass substrates. The XRD technique is suitable for different structural analyses of these thin films.

The XRD (X-ray diffraction) technique is generally used to determine the micro structural parameters /15/ such as crystalline size, r.m.s. strain, dislocation density, stacking fault probability, crystal structure, strain and composition. Work on structural studies of vacuum evaporated II-VI compound thin films by XRD technique have been reported by many workers /16-21/.

XRD, especially the powder diffraction method is generally preferred for its simplicity. It is very effective for quantitative analysis of various imperfections and other crystallographic features. Of course for inherent low scattering and high penetrating power of X-rays, XRD technique is not very suitable for the analysis of surface structure of thinner films. For films having thickness greater than 1000Å, the XRD technique is generally employed to obtain a whole range of information about the crystallographic aspects of thin films. From XRD analysis information regarding lattice parameters, orientations of crystal plans, grain size, lattice structure (i.e. epitaxial, polycrystalline, amorphous etc), defects and stress in thin films can be obtained. Estimation of different defects such as twining, anti phase structure etc are also been reported /22-24/. The mechanical stability of a thin film plays a major role for designing different electronic

devices. So study of thermal and intrinsic stress and strain of thin films /25,26/ is also an area of considerable interest. Several workers /27-29/ have studied the structural characterization of II-VI compounds thin films and their correlation with other properties. Optoelectronic properties of II-VI thin films are sensitive to the microstructural parameters. A correlative study between the optoelectronic properties and structural attributes is an area of considerable importance so far as the optoelectronic devices are concerned.

3.2 Experimental

The thin films for XRD analysis were deposited together with other films for optoelectronic measurements in a single run under identical growth conditions so that all the films are of the same thickness and possess identical structural characteristics. These films were deposited on the glass substrates of size as per specification of the specimen holder of the X-ray diffractometer. A brief discussion regarding the experimental techniques of XRD method is made in chapter II.

For studying degree of crystallization and to identify phases X-ray diffraction patterns of different films were observed using Phillips X-ray diffractometer (PIHILIPS X'PERT PLUS). During the X-ray scan monochromatic CuKα radiation of wavelength 1.54056Å was used and the generator was operated at 40 KV and 30 mA. Care was taken to minimize the instrumental broadening by using servo controlled highly stabilized power supply. Automatic programmable silt adjustment system was used to reduce divergence. Routine check of calibration and adjustment of the instrument was carried out with standard sample. P.C. based data acquisition and dated processing systems were used. The final diffraction patterns were recorded by suitably suppressing the noise levels. For the calculation of grain size with better accuracy the prominent peaks were amplified by computer programming from which the peak widths at half maxima readings were taken. The line profile were chart recorded at a scanning rate $(0.01)^0$ s^{-1} with Philips automatic recorder. The diffraction spectra of powder sample and thin films under different conditions were analyzed using Philips X'pert software. The spectrum of the power fresh sample was used as the standard to make comparisons with the spectra of thin films. The experimental XRD data, which were recorded for a film or bulk sample,

were the angular position (2θ) of peaks, inter planner distance, total diffracted intensity, back ground intensity, intensity ratios with respect to highest peak and the peak significance for each peak.

3.3 X-Ray Diffraction

When a monochromatic parallel beam of X-ray impinges on a crystal, the crystal lattice diffract the beam to produce interference pattern, the nature of which can be explained by the Bragg's law /30/

$$|(\vec{S} - \vec{S}_o) / \lambda| = |\vec{H}_{hkl}| \tag{3.1}$$

where $\vec{S}$ and $\vec{S}_o$ are unit vectors in the directions of primary and the diffracted beams. The vector $\vec{H}_{hkl}$ is perpendicular to the planes [hkl] and whose magnitude is reciprocal of the inter-planner spacing d_{hkl} of the set of lattice planes [hkl].

The equation (3.1) is equivalent to the usual form of Bragg's law

$$n\lambda = 2\, d_{hkl} \sin\theta \tag{3.2}$$

where θ is the Bragg's angle made by the vectors $\vec{S}/\lambda$ or $\vec{S}_o/\lambda$ with the diffracting plane.

The locus of the diffracted beam from a set of planes with same inter planner spacing lies on a cone with half apex angle 2θ (the angle the between incident and the diffracted beam). Similarly the diffracted beams from other sets of lattice planes with different inter planer spacing d_1, d_2, d_3, ...etc also lie along different cones with half apex angles $2\theta_1$, $2\theta_2$, $2\theta_3$ .....etc. These cones would be coaxial since the incident beam direction remains the same for all these lattice planes.

For a polycrystalline material the intensity, I, of a diffracted X-ray beam is given by the relation /31/

$$I \propto F^2 \times P \left[\frac{1+\cos^2 2\theta}{\sin^2\theta \cos\theta}\right] \tag{3.3}$$

where F is the structure factor, P is a multiplying factor; which is the number of equivalent planes of direction [hkl] that take part in the diffraction processes.

Generally the principal phase structure of II-IV compound thin films is usually of cubic ZnS or hexagonal Wurtzite type. Sometimes it possesses mixed structure also with presence of both the phases depending upon the growth conditions /32-34/. In the present study the phase structure of the thermally evaporated CdSe thin films are determined by comparing the peak positions of the XRD profiles of thin films and that of the fresh samples, with the standard JCPDS X-ray powder file data of the material.

Determination of lattice constant: The inter planer spacing of a [hkl] set of planes of a cubic lattice of lattice parameter, a, is given by /35/

$$d_{hkl} = \frac{a}{\sqrt{h^2 + k^2 + l^2}} = a / \sqrt{N} \tag{3.4}$$

where $N = h^2+k^2+l^2$ is a number. Observing the distribution of N values, the type of the cubic lattice may be determined /36,37/.

Hence from the Bragg's law it implies that

$$\mathrm{Sin}^2\theta = \frac{\lambda^2}{4a^2}\left(h^2 + k^2 + l^2\right) = \frac{\lambda^2}{4a^2} N \tag{3.5}$$

For hexagonal crystals the lattice constants, a, and, c, can be evaluated from the following relations /38/

$$\frac{1}{d^2} = \frac{4}{3}\left(\frac{h^2 + hk + k^2}{a^2}\right) + \frac{l^2}{c^2} \tag{3.6}$$

and from Bragg's law

$$\mathrm{Sin}^2\theta = \frac{\lambda^2}{3a^2}\left(h^2 + k^2 + l^2\right) + \frac{\lambda^2}{4c^2} l^2 \tag{3.7}$$

According to Vegards law, the lattice parameters of hexagonal unit cell are nearly related to cubic lattice parameters of same material by /39, 40/

$$a_{hex} = \left(\tfrac{1}{2}\right)^{1/2} a_{cubic} \qquad \text{and} \qquad c_{hex} = \left(\tfrac{4}{3}\right)^{1/2} a_{cubic} \tag{3.8}$$

Hence for ideal Wurtzite lattice, the relation between the two lattice parameters is

$$c_{hex} = (1.633)a_{hex} \tag{3.9}$$

which may be used for the calculation of lattice parameters of CdSe thin films.

Grain Size: The grain size (D_{hkl}) for the thermally evaporated CdSe thin films are evaluated for the most preferred plane [hkl] using the Scherrer formula /41/

$$D_{hkl} = \frac{K\lambda}{\beta_{2\theta}\cos\theta} \tag{3.10}$$

where θ is the Bragg's angle, λ is the wavelength of X-rays used, $\beta_{2\theta}$ is the width of the peak at the half of the maximum peak intensity. k is a proportionality constant whose value is taken as 0.94. Apart from the principal peak, if there be any other peak in the XRD pattern then the corresponding grain size is also evaluated, using the same formula.

Average strain: The origin of strain is related to lattice 'mis-fit' which in turn depends upon the growing conditions. The microstrain developed in thin film is calculated from the relation /42/

$$\varepsilon_{hkl} = \frac{\beta_{2\theta}\cot\theta}{4} \tag{3.11}$$

where θ is the Bragg's angle. Using this relation magnitude of lattice strain, ε_{hkl}, along the preferred orientations, is calculated for films deposited at different T_s and having different thickness.

Dislocation Density: Dislocations are an imperfection in a crystal associated with misregistry of the lattice in one part of the crystal with respect to another part. Unlike vacancies and interstitial atoms, dislocations are not equilibrium imperfections /43, 44/. In fact growth mechanism involving dislocation is a matter of importance. The dislocation density of thin films are given by the Williamson and Smallman's relation /45,46/

$$\delta = n/D^2 \tag{3.12}$$

where n is a factor, which equals unity giving minimum dislocation density and D is the grain size.

Using this relation, the magnitude of dislocation density was calculated along different orientations for the films deposited at different T_s and for films having thickness of different order.

Accurate measurement of lattice parameter: Accurate measurements of lattice parameters are necessary for the crystallographic characterization of thin films. There are several possible sources of error like divergences of X-ray beams, refraction and absorption of X-rays by the specimens etc in the measurement of θ and d values. So accuracy in the determination of lattice constant is dependent upon the accuracy of their measurements. We have

$$d = \frac{\lambda}{2}\operatorname{cosec}\theta \tag{3.13}$$

So $$\delta d = -\frac{\lambda}{2}\left(\operatorname{cosec}\theta \cot\theta\right)\delta\theta$$

For $$\theta = 90^{\circ},\ \delta d/d = 0$$

Therefore measurement of lattice parameters is most accurate when the corresponding evaluation is extrapolated to $\theta = 90^{\circ}$. Usually the Nelson-Riley plot /47/ is used for this purpose. It is plot between the calculated lattice constant values for different planes and the error function /48/

$$f(\theta) = \frac{1}{2}\left(\cos^2\theta/\sin\theta + \cos^2\theta/\theta\right) \tag{3.14}$$

3.4 Structural Analysis

3.4.1 X-ray diffractogram of CdSe bulk sample

CdSe bulk samples were procured from M/S Koch Light Lab. England, and used for electrical, optical as well as structural analysis in thin film form. The coarse grained sample was crushed to fine power form and the same fine powder of CdSe was analyzed by way of X-ray diffraction technique to identify the structural phases. Fig 3.1 shows

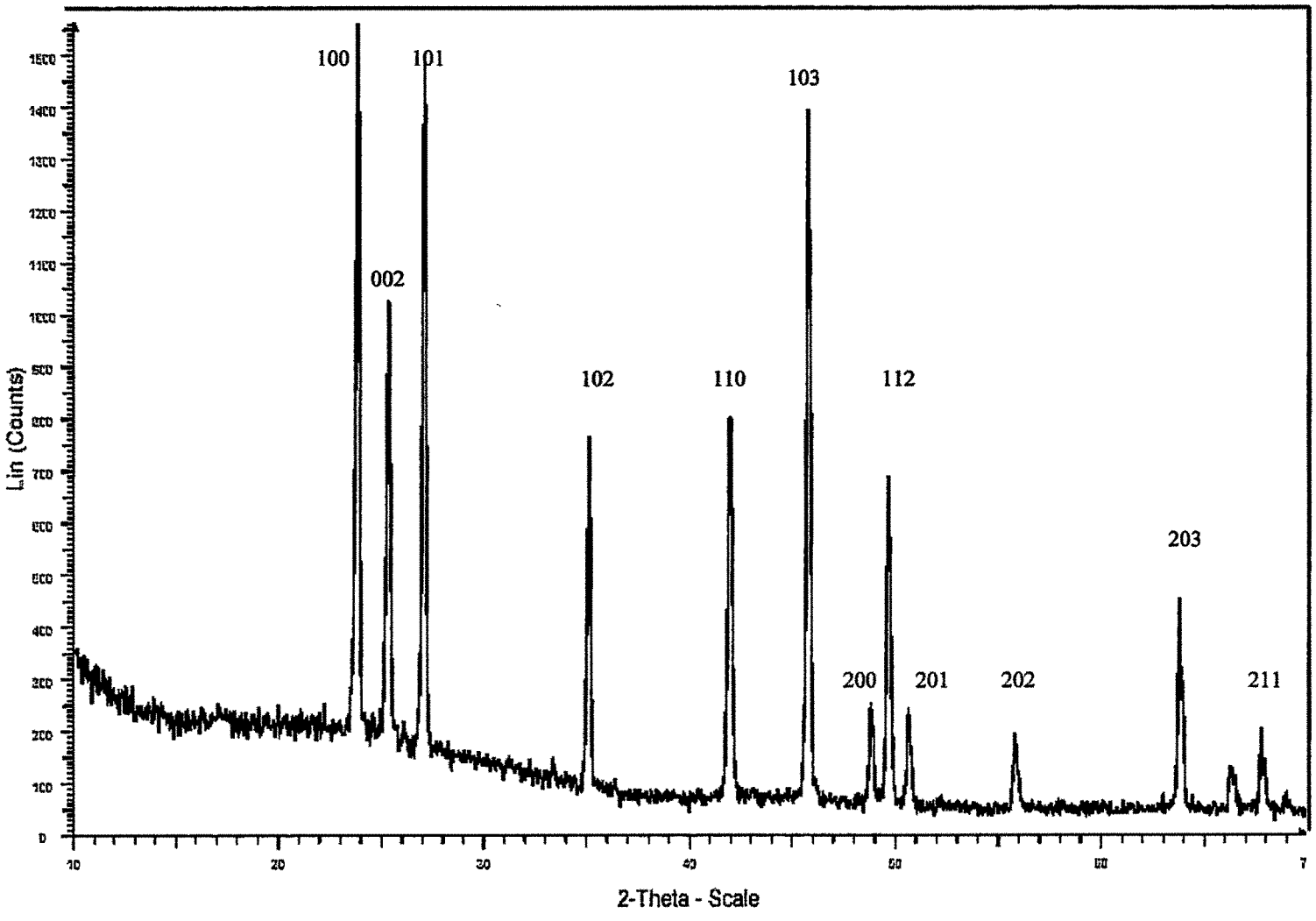

Figure 3.1 X-ray diffractogram of bulk Cadmium Selenide (CdSe) sample.

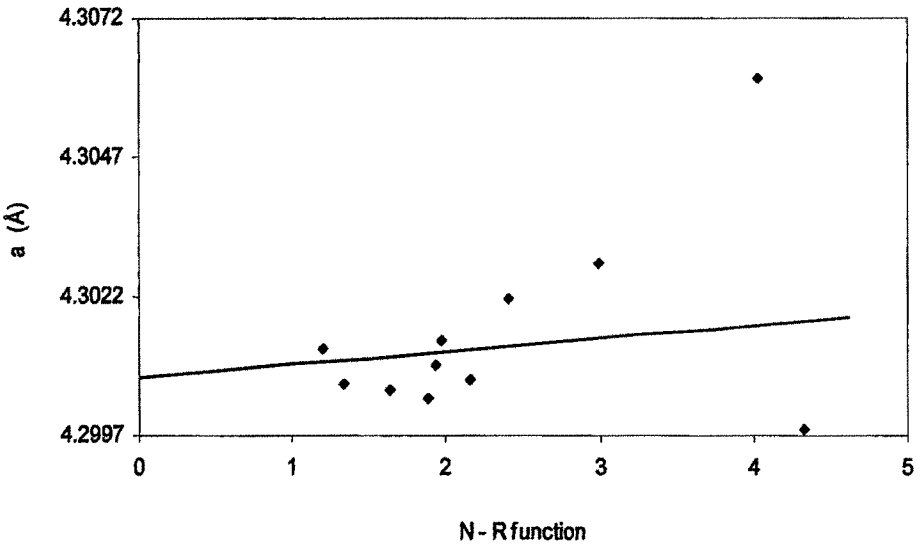

Figure 3.2(a) Nelson – Riley plot of CdSe bulk sample for lattice parameter, a.

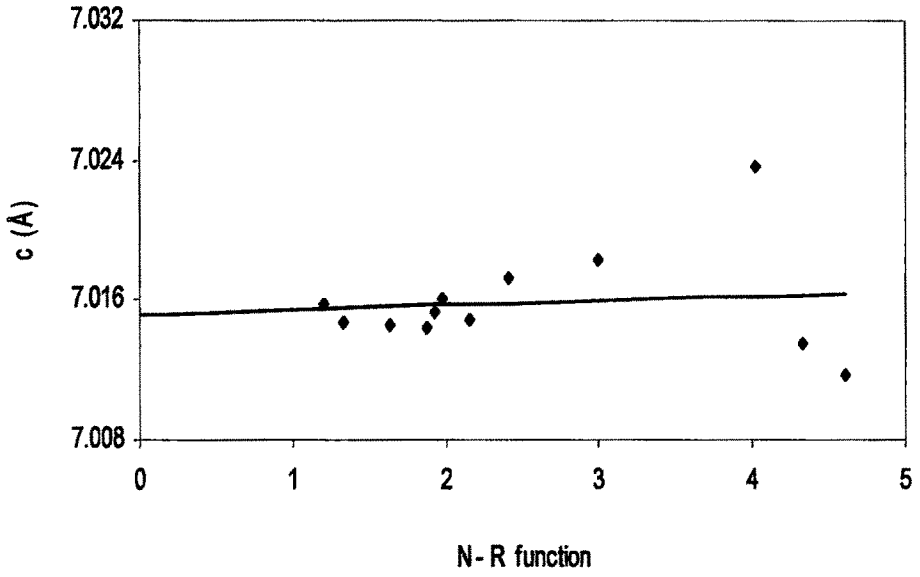

Figure 3.2(b) Nelson – Riley plot of CdSe bulk sample for lattice parameter, c.

the X-ray diffraction line profiles of the powder sample material. The peaks at 2θ values obtained from the powder diffractogram of CdSe are shown in the Table 3.1 corresponding to diffraction from different planes of the hexagonal phase. The exhibited peak positions and the, d, values, are found to be in close proximity to the corresponding values of JCPDS (Joint Committee for Powder Diffraction Standard) file data /49/ for hexagonal CdSe. No extra peaks are observed expect those mentioned in the JCPDS file data for hexagonal CdSe sample. Hence it is ascertained that CdSe sample powder used as the source material to deposit films is in hexagonal phase and stochiometric in composition. Using equation (3.7) for the orientation of [100] plane at, $2\theta = 23.87^0$, the value of lattice parameter, a, is found to be 4.299Å and using the same equation for the orientation of [002] plane at $2\theta = 25.30^0$ value for the lattice parameter, c, is calculated as 7.013Å.

Therefore in these cases in order to find the values of, a, and, c, for other planes instead of using equation (3.9) the following relation is used.

$$c_{hex} = (7.013/4.299)\, a_{hex} = 1.631\, a_{hex} \qquad (3.10)$$

The calculated values of, a, and, c, are close to those cited in the literature /50, 51/. These calculated values of, a, and, c, for all the observed planes in the powder diffractogram of CdSe sample are systematically presented in Table 3.1.

The corrected values of the lattice constants, a, and, c, of the sample are estimated from Nelson-Riley plots shown in Fig 3.2(a) and Fig 3.2(b). The values are found to be 4.3007 Å and 7.0150 Å for, a, and, c, respectively which are close to the JCPD standard 4.299Å and 7.010Å.

3.4.2 Analysis of diffractogram of CdSe thin films

The XRD line profiles of CdSe thin films, of different thickness but grown at same T_s and also for films of same thickness but deposited at different T_s, were studied for the purpose of structural analysis. For all the films rest of the deposition parameters were kept constant. It was observed that thin films of CdSe grown at room temperature were amorphous (Fig 3.4) and those grown at elevated T_s (from 473 to 623K) were polycrystalline in nature. Figs 3.3(a to d) show the XRD pattern of four CdSe thin films

Table 3.1 X-ray diffractogram data of bulk Cadmium Selenide sample.

[hkl] values from JCPDS data	d(Å) values from JCPDS data	Observed values of d(Å)	Observed $(2\theta)^0$ values of peaks	Calculated values of a(Å)	Calculated values of c(Å)
100	3.720	3.732	23.87	4.299	7.011
002	3.516	3.517	25.302	4.299	7.013
101	3.290	3.295	27.038	4.306	7.023
102	2.554	2.555	35.086	4.302	7.018
110	2.151	2.152	41.950	4.302	7.017
103	1.980	1.981	45.764	4.300	7.014
200	1.861	1.863	48.838	4.301	7.016
112	1.834	1.834	49.670	4.300	7.015
201	1.800	1.800	50.661	4.300	7.014
202	1.645	1.645	55.832	4.300	7.014
203	1.456	1.457	63.823	4.300	7.014
211	1.380	1.380	67.806	4.301	7.015

of equal thickness 2000Å, deposited at four different T_s = 623K, 573K, 523K and 473K respectively. Figs 3.5(a to d) show XRD patterns of another four CdSe films of thickness respectively 2230Å, 1750Å, 1530Å and 1000Å, deposited at T_s = 473K.

The broad hump that is observed in the background of XRDs of thin films is due to the amorphous glass substrate and also possibly due to some amorphous phase present in the CdSe thin films. Figs 3.6(a to c) show the amplified XRD spectra of the prominent peak, of the corresponding XRDs, of the three CdSe thin films presented in Figs 3.5(b to d) respectively. From these amplified patterns the respective half of the maximum peak intensity (FWHM) is evaluated.

From the JCPDS X-ray powder file data comparing observed, d, values of the XRD patterns of the films with the standard, d, values, it was concluded that all the CdSe thin films deposited within the elevated T_s range, from 473 to 623K, are of hexagonal ZnS type structure.

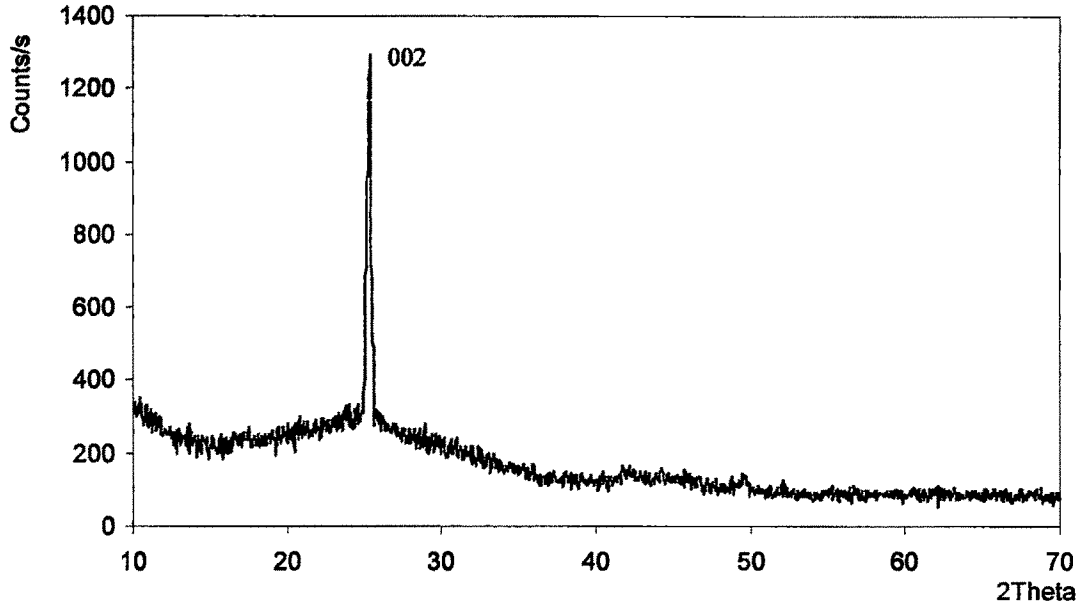

Figure 3.3(a) X-ray diffractogram of a CdSe thin film (t = 2000Å) grown at T_s = 623K.

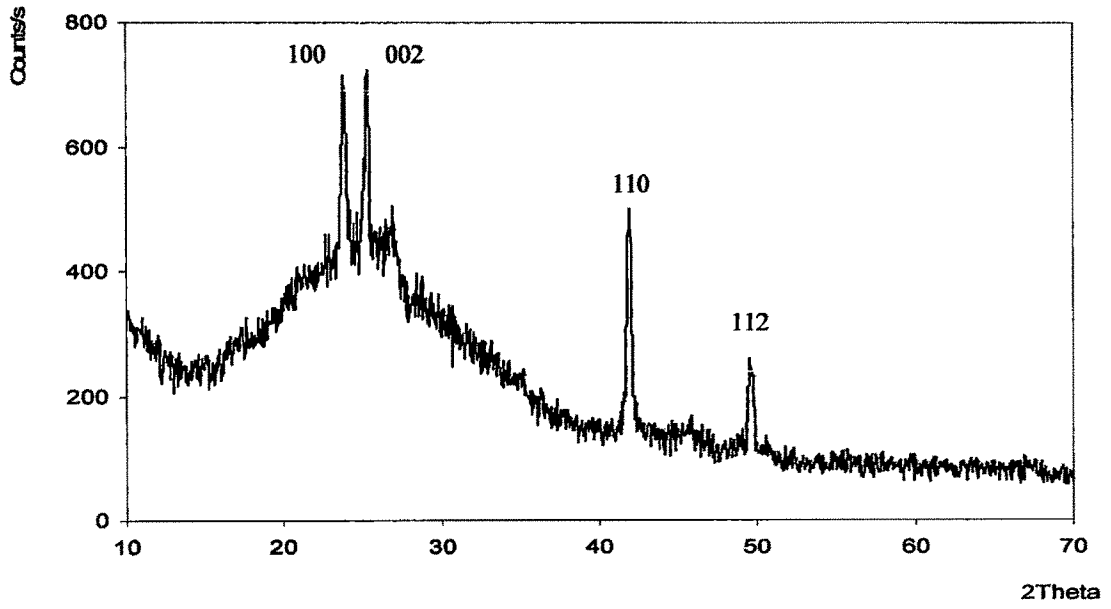

Figure 3.3(b) X-ray diffractogram of a CdSe thin film (t = 2000Å) grown at T_s = 573K.

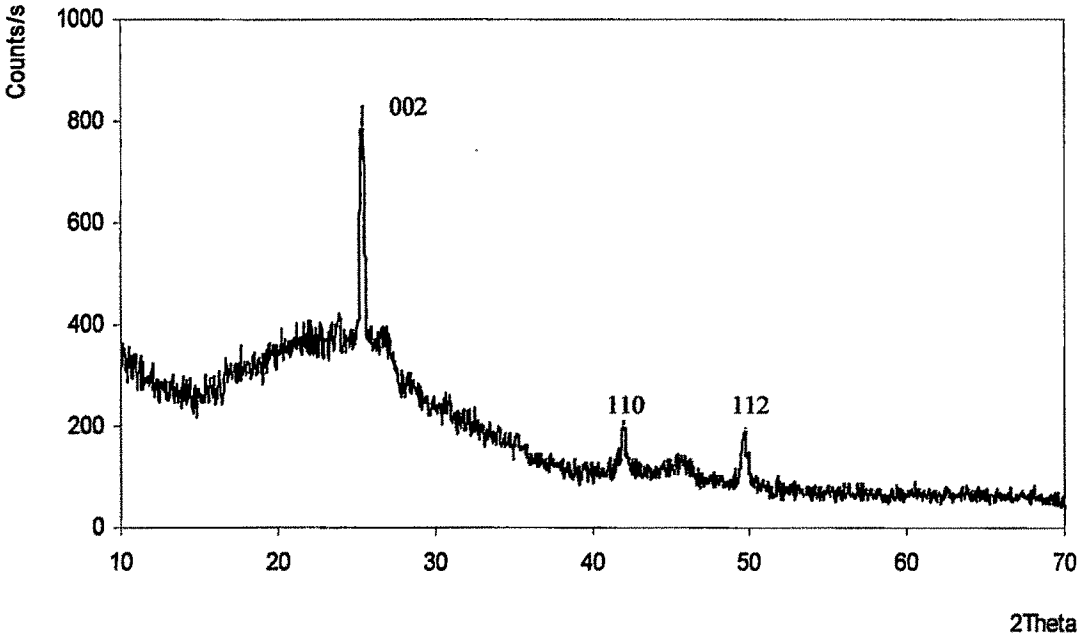

Figure 3.3(c) X-ray diffractogram of a CdSe thin film (t = 2000Å) grown at T_s = 523K.

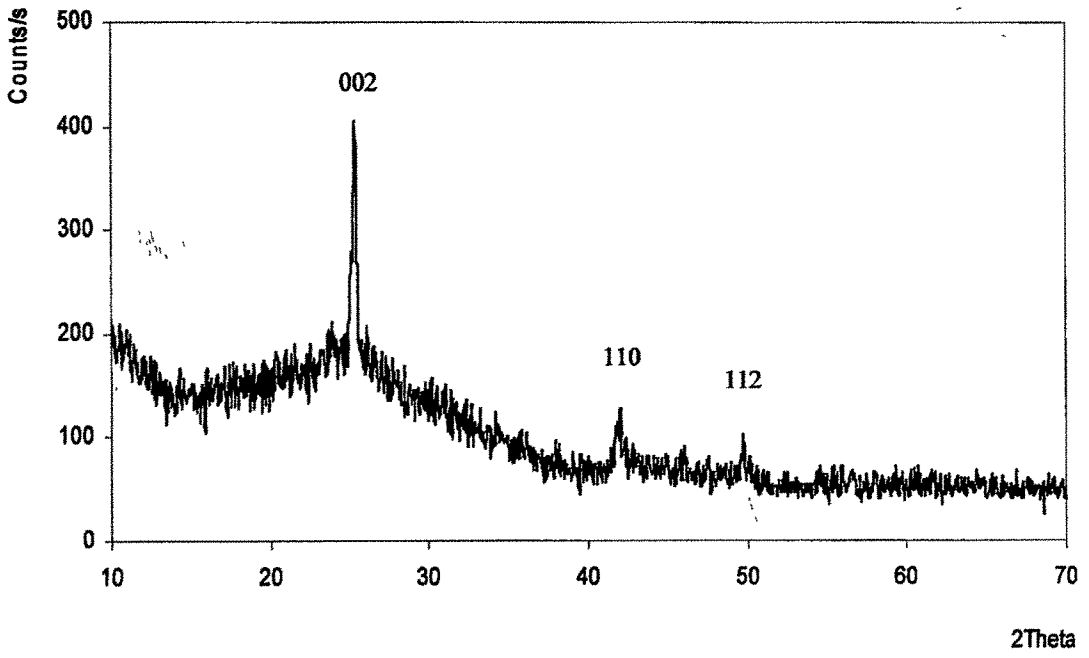

Figure 3.3(d) X-ray diffractogram of a CdSe thin film (t = 2000Å) grown at T_s = 473K.

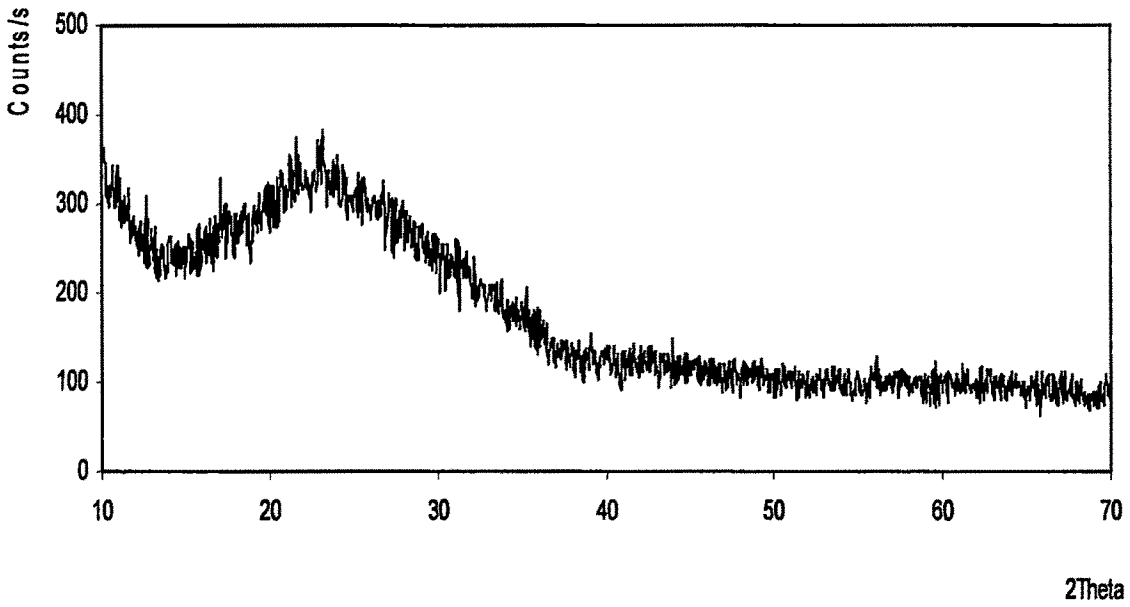

Figure 3.4 X-ray diffractogram of a CdSe thin film (t = 2000Å) grown at T_s = 300K.

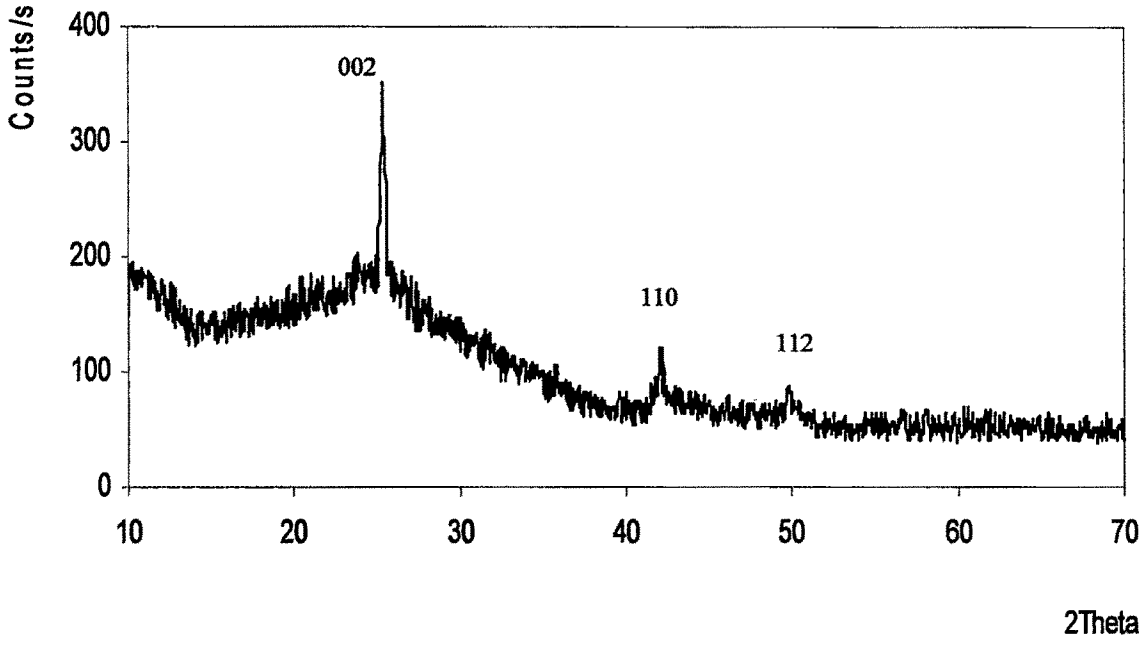

Figure 3.5(a) X-ray diffractogram of a CdSe thin film (t = 2230Å) grown at T_s = 473K.

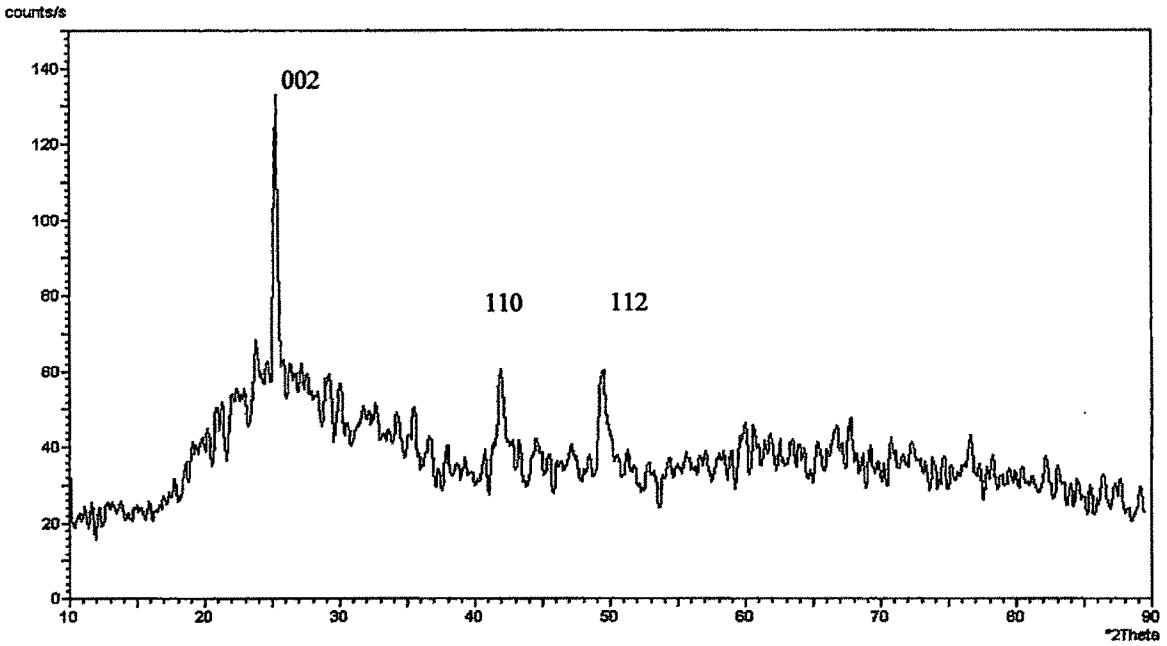

Figure 3.5(b) X-ray diffractogram of a CdSe thin film (t = 1750Å) grown at T_s = 473K

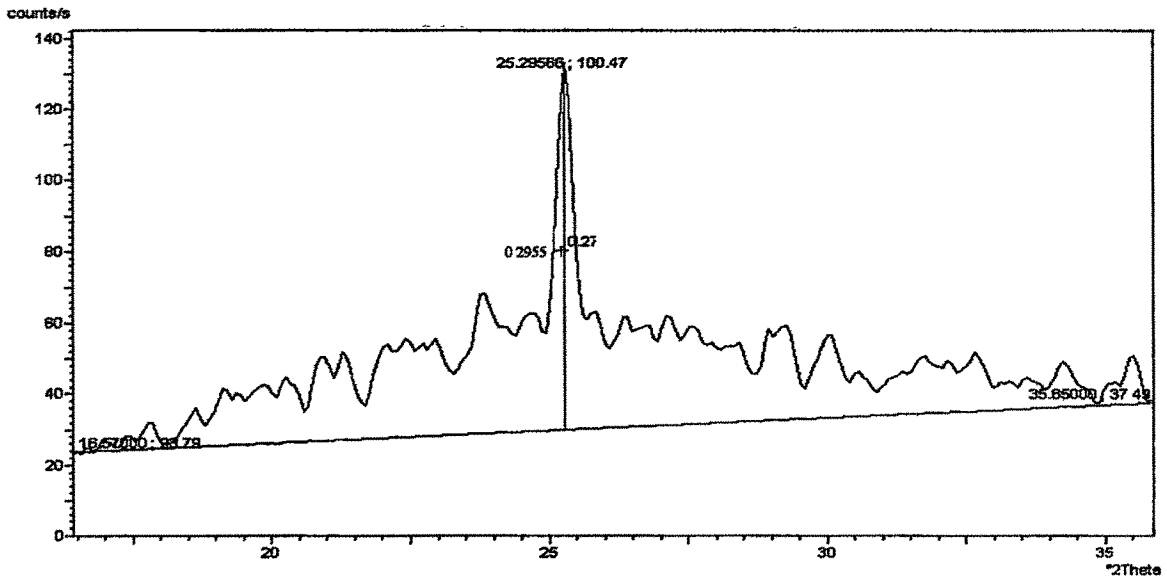

Figure 3.6(a) FWHM of [002] peak of a CdSe film (t = 1750Å) grown at T_s = 473K.

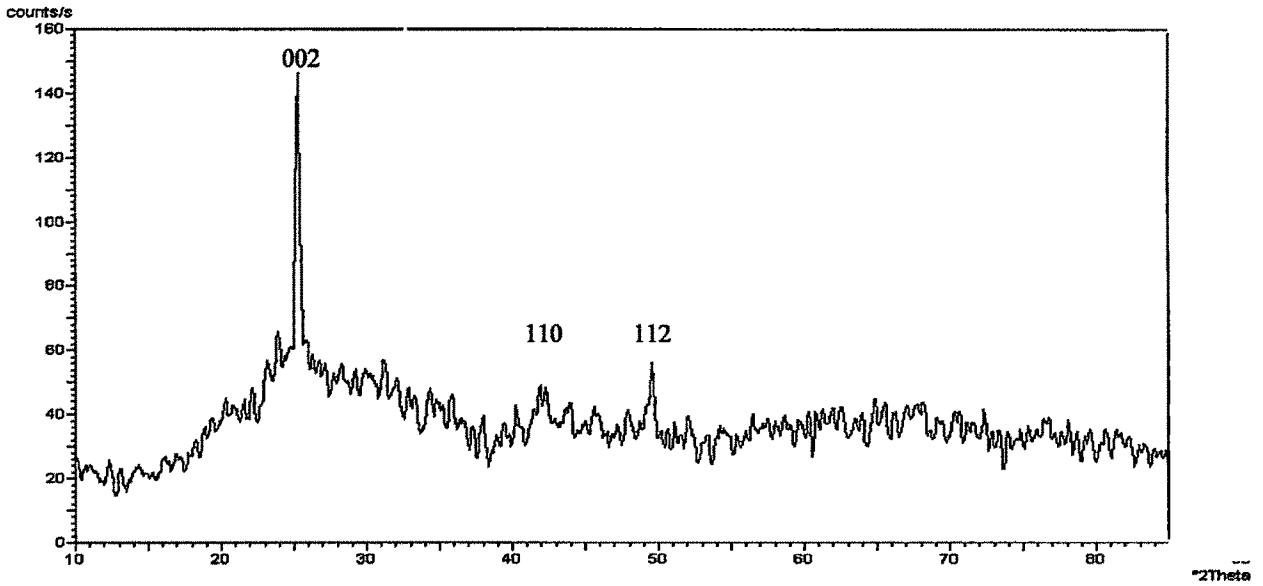

Figure 3.5(c) X-ray diffractogram of a CdSe thin film (t = 1530Å) grown at T_s = 473K.

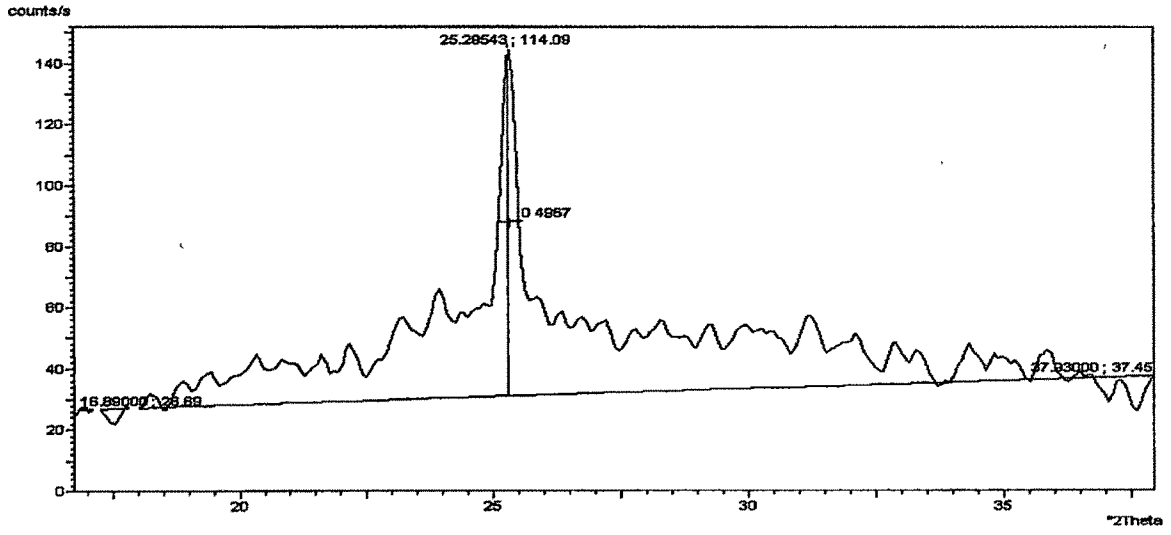

Figure 3.6(b) FWHM of [002] peak of a CdSe film (t = 1530Å) grown at T_s = 473K.

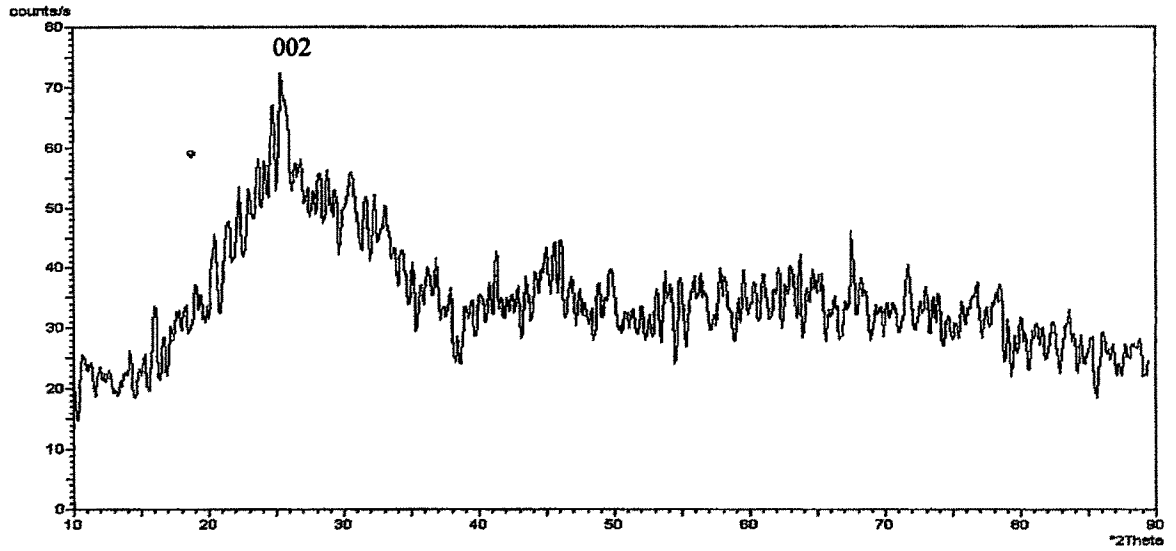

Figure 3.5(d) X-ray diffractogram of a CdSe thin film (t = 1000Å) grown at T_s = 473K.

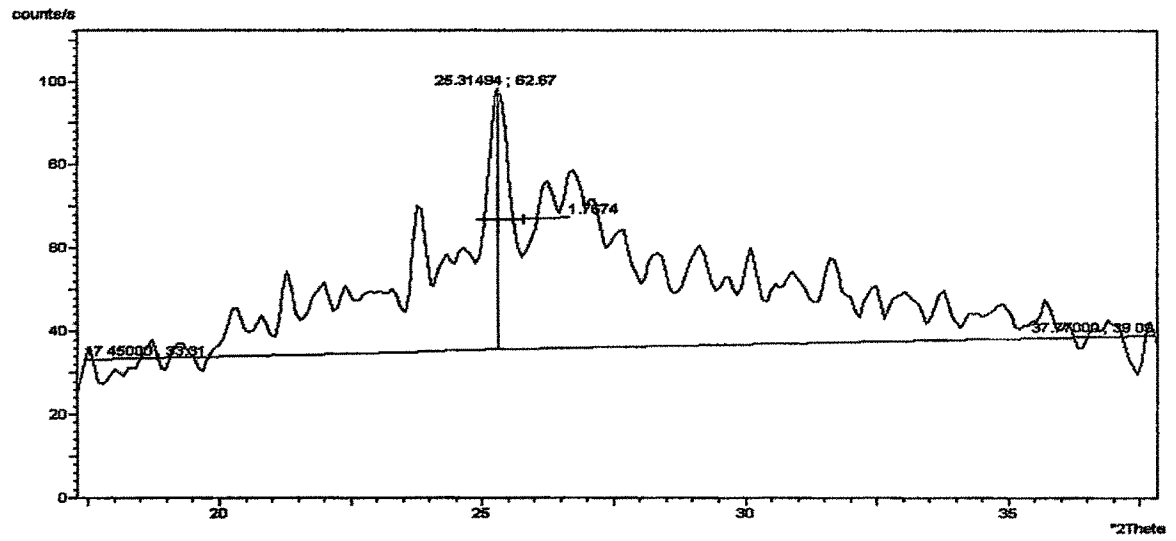

Figure 3.6(c) FWHM of [002] peak of a CdSe film (t = 1000Å) grown at T_s = 473K.

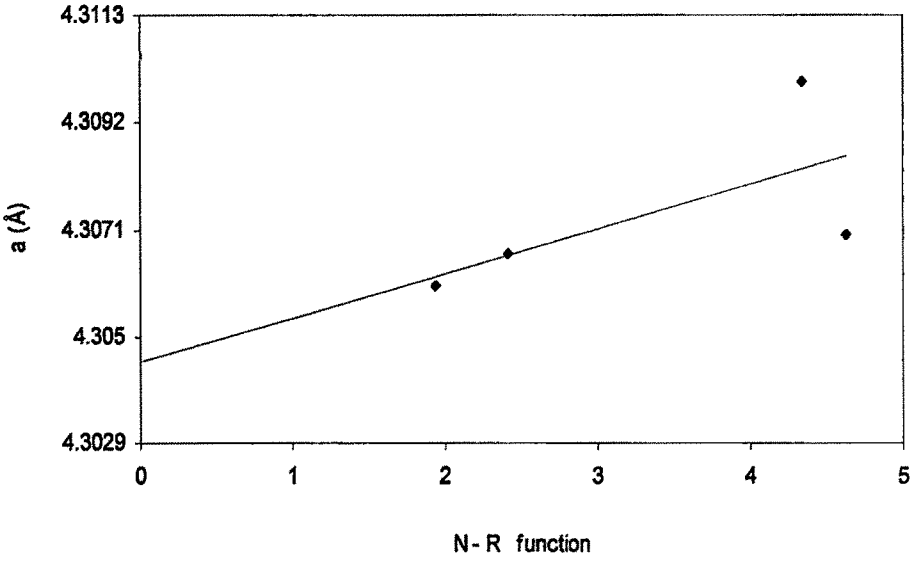

Figure 3.7(a) Nelson – Riley plot of a CdSe thin film (t = 2000Å, T_s = 573K) for lattice constant, a.

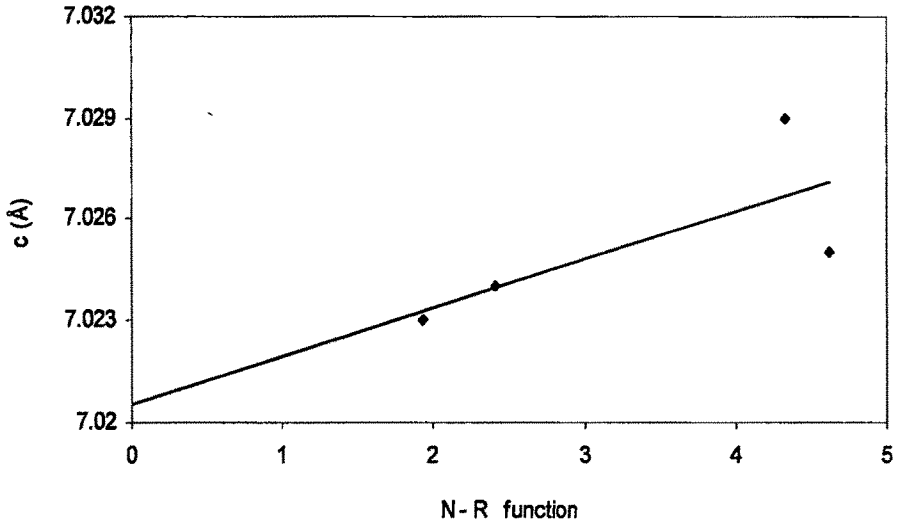

Figure 3.7(b) Nelson – Riley plot of a CdSe thin film (t = 2000Å, T_s = 573K) for lattice constant, c.

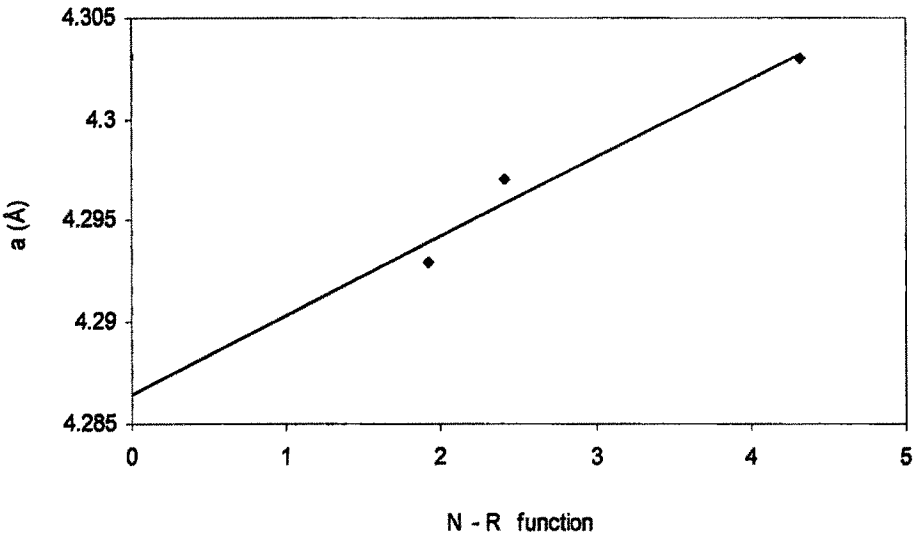

Figure 3.7(c) Nelson – Riley plot of a CdSe thin film (t = 2000Å, T_s = 473K) for lattice constant, a.

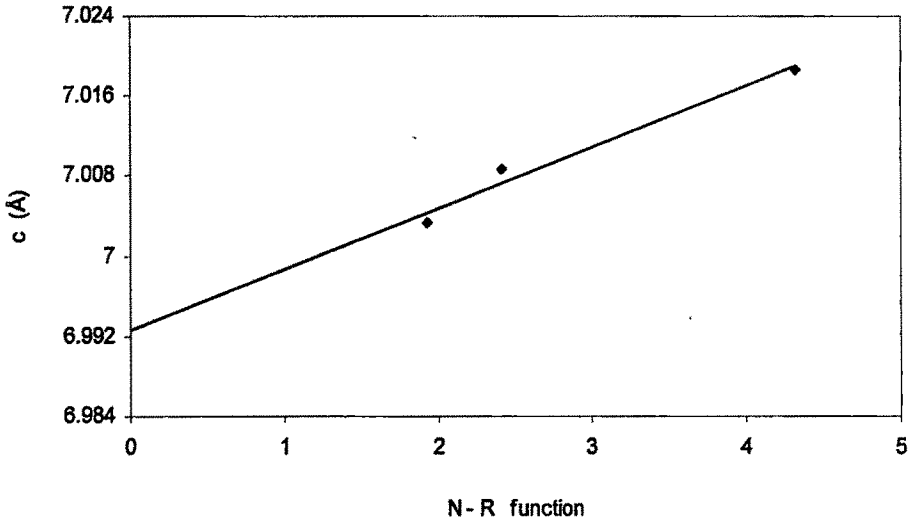

Figure 3.7(d) Nelson – Riley plot of a CdSe thin film (t = 2000Å, T_s = 473K) for lattice constant, c.

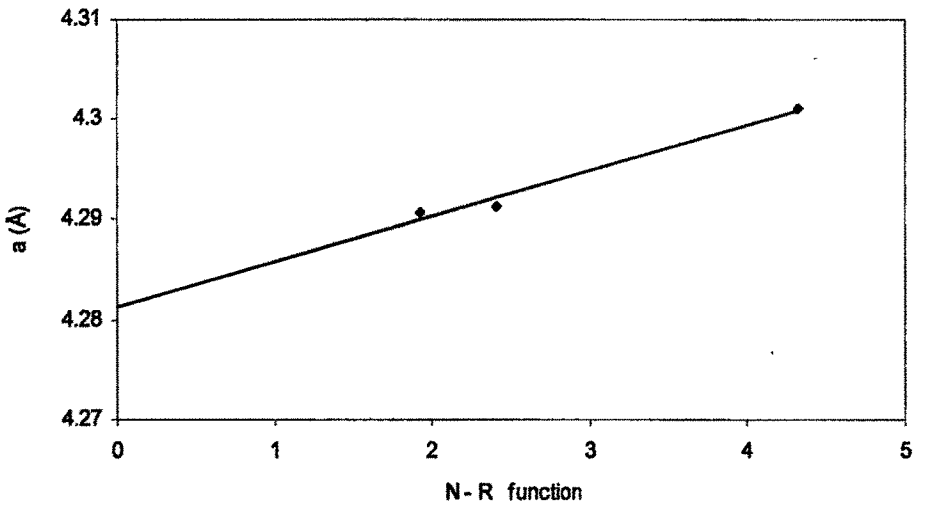

Figure 3.7(e) Nelson – Riley plot of a CdSe thin film (t = 2230Å, T_s = 473K) for lattice constant, a.

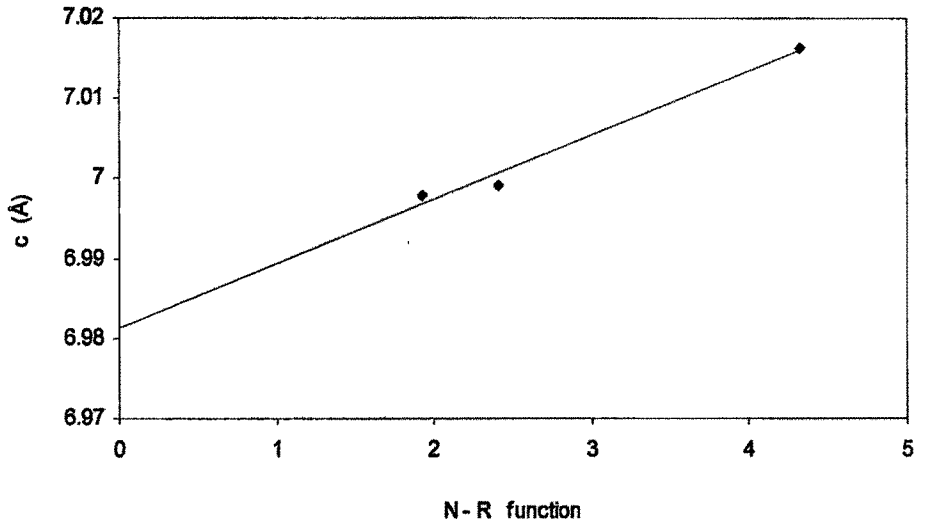

Figure 3.7(f) Nelson – Riley plot of a CdSe thin film (t = 2230Å, T_s = 473K) for lattice constant, c.

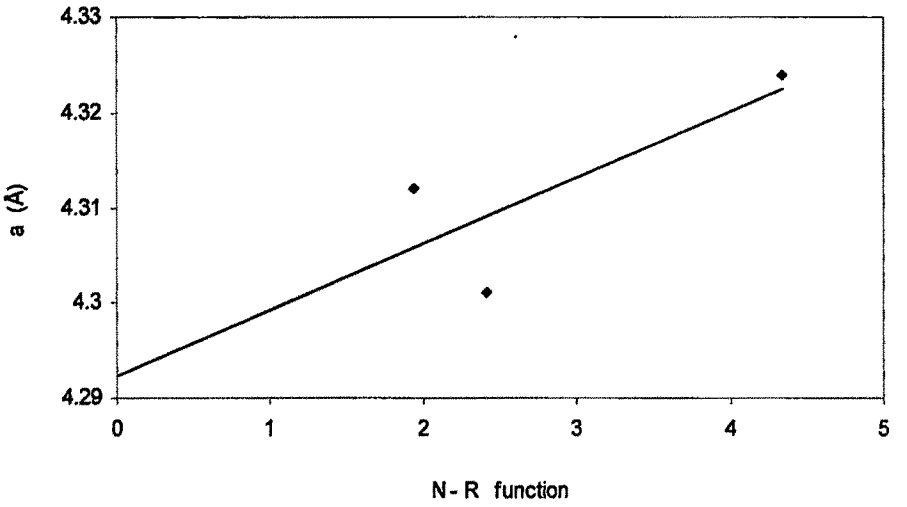

Figure 3.7(g) Nelson – Riley plot of a CdSe thin film (t = 1750Å, T_s = 473K) for lattice constant, a.

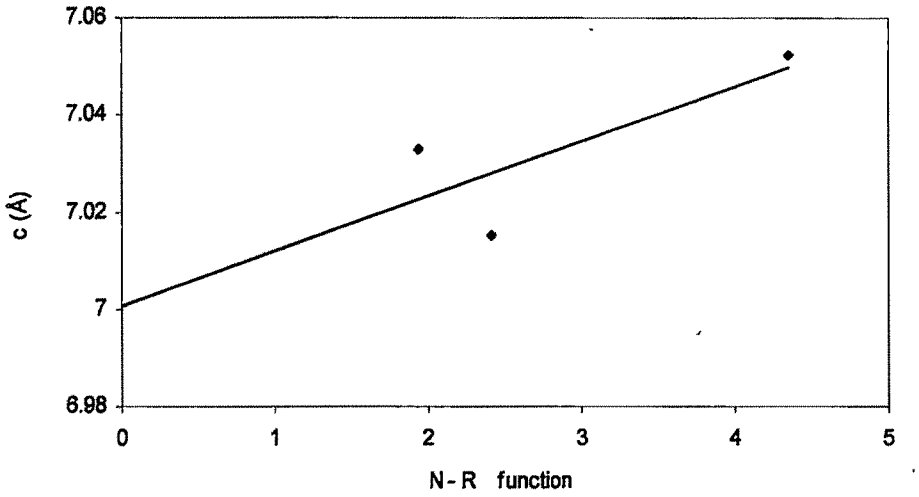

Figure 3.7(h) Nelson – Riley plot of a CdSe thin film (t = 1750Å, T_s = 473K) for lattice constant, c.

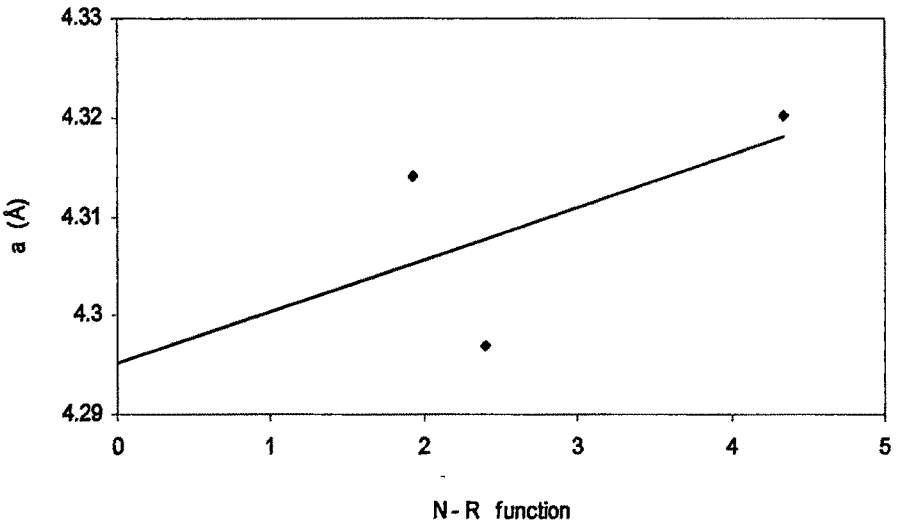

Figure 3.7(i) Nelson – Riley plot of a CdSe thin film (t = 1530Å, T_s = 473K) for lattice constant, a.

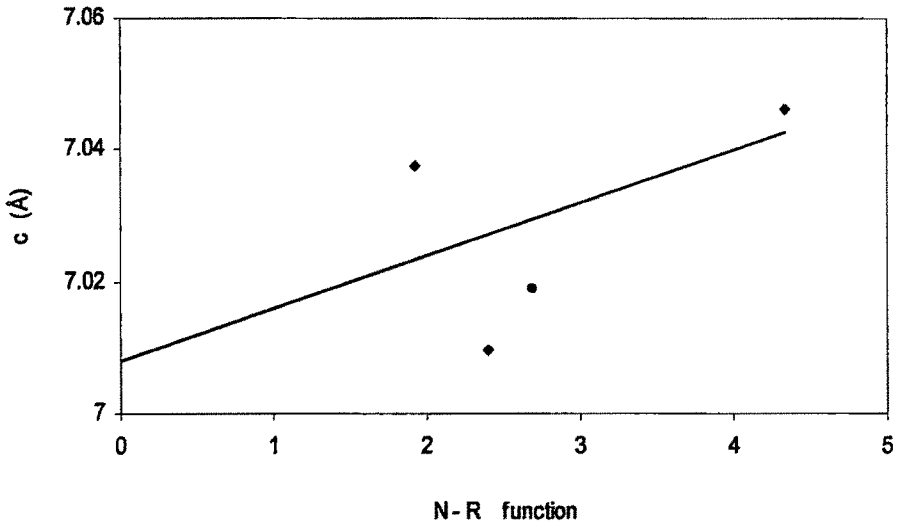

Figure 3.7(j) Nelson – Riley plot of a CdSe thin film (t = 1530Å, T_s = 473K) for lattice constant, c.

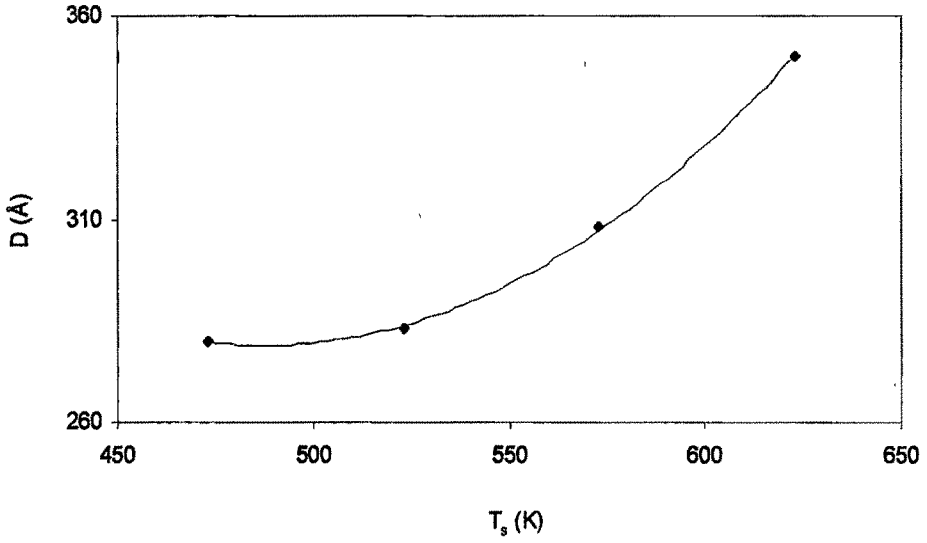

Figure 3.8(a) Variation of grain size (D) with T_s ,of CdSe thin films of constant t = 2000Å.

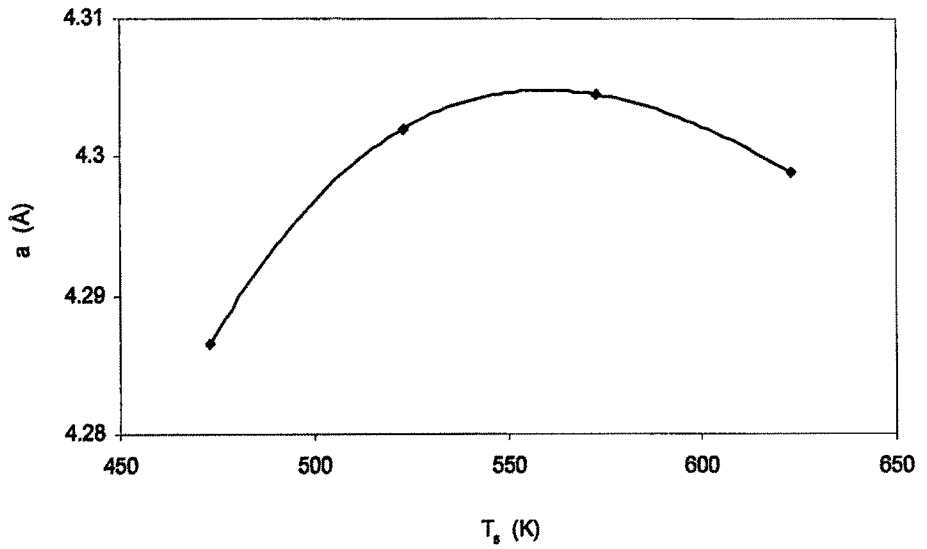

Figure 3.8(b) Variation of lattice constant, a, with T_s ,of CdSe thin films of constant t = 2000Å.

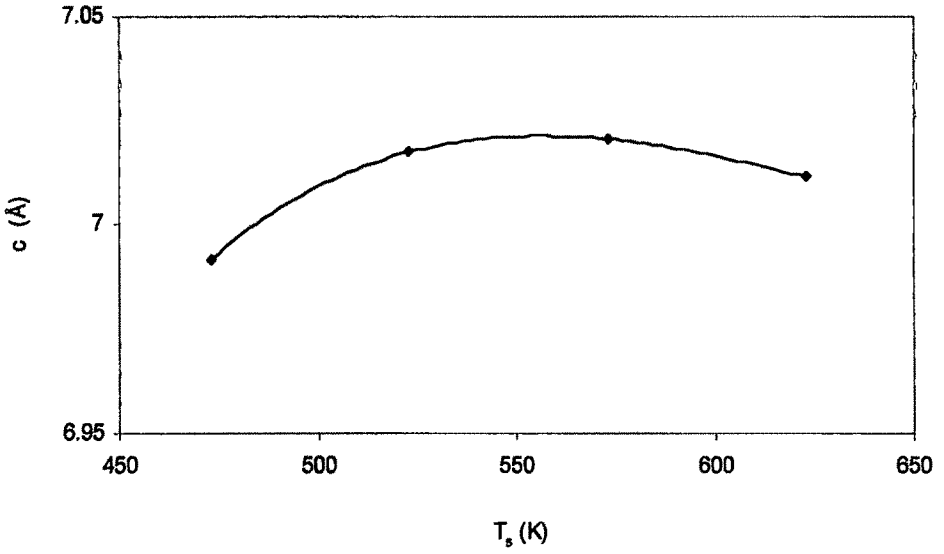

Figure 3.8(c) Variation of lattice constant, c, with T_S ,of CdSe thin films of constant t = 2000Å.

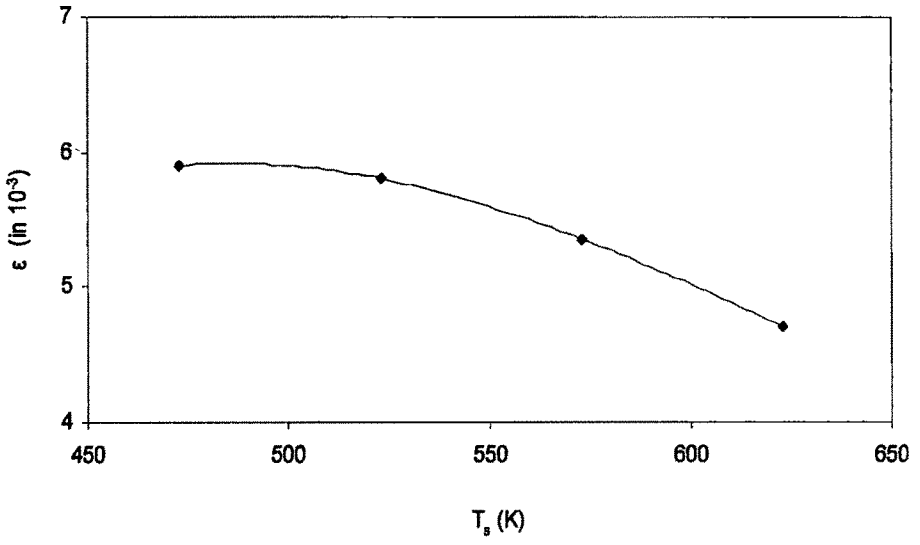

Figure 3.8(d) Variation of strain (ε) with T_S ,of CdSe thin films of constant t = 2000Å.

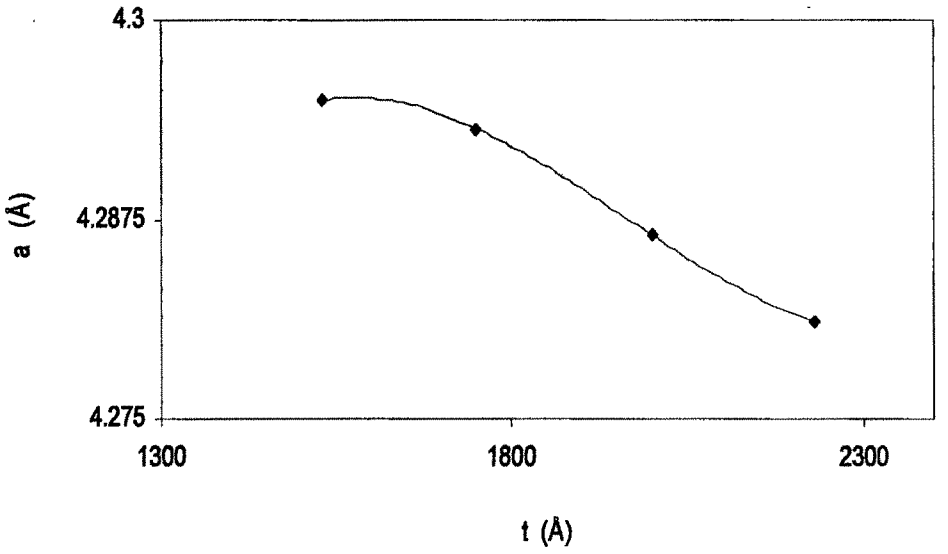

Figure 3.9(a) Variation of lattice constant, a, with thickness of CdSe thin films grown at elevated $T_s = 473K$.

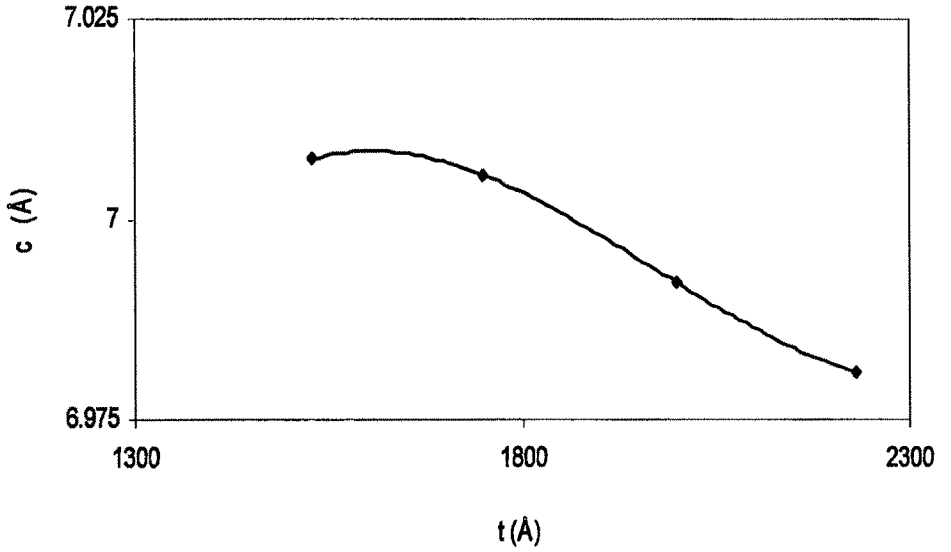

Figure 3.9(b) Variation of lattice constant, c, with thickness of CdSe thin films grown at elevated $T_s = 473K$.

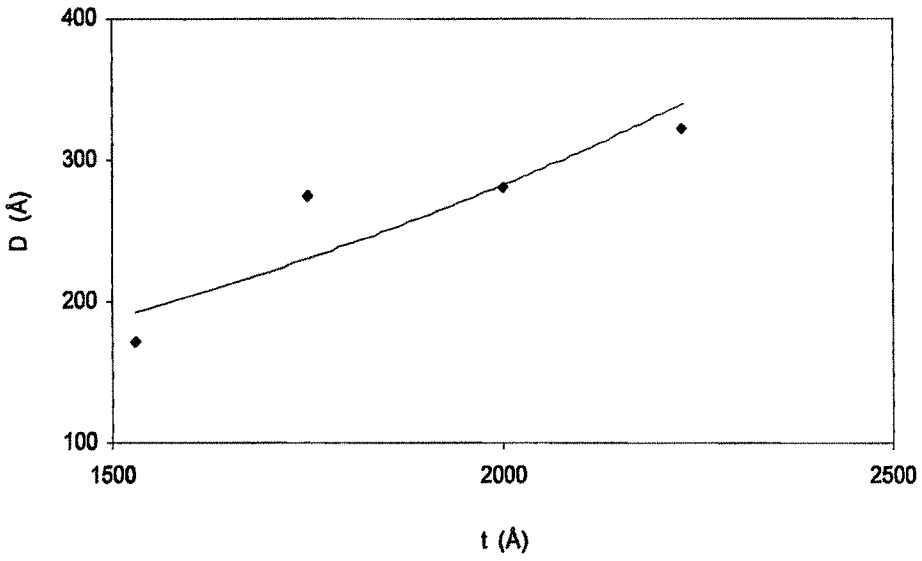

Figure 3.9(c) Variation of grain size (D) with film thickness of CdSe thin films (t) grown at elevated $T_s = 473K$.

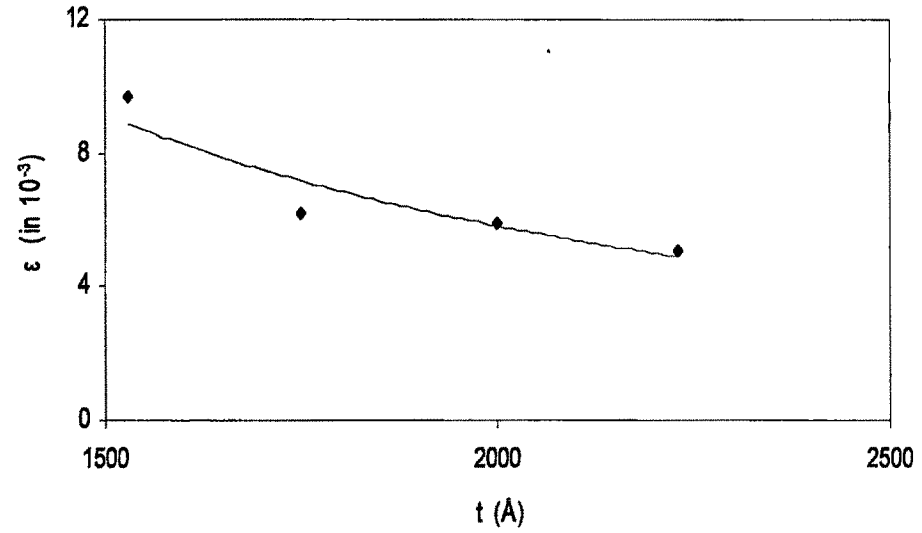

Figure 3.9(d) Variation of strain (ε) with film thickness of CdSe thin films grown at elevated $T_s = 473K$.

Table 3.2 d_{hkl} values of CdSe sample obtained from JCPDS standard, d_{hkl} & 2θ values obtained from source material and from CdSe thin films, of t = 2000Å, grown at different, T_s as well as from CdSe thin films of different, t, deposited at same T_s = 473K, corresponding to different lattice planes.

Lattice planes	d_{hkl} & $(2\theta)^o$	100	002	110	112
JCPD standard	d_{hkl}	3.720	3.516	2.151	1.834
Source material	d_{hkl}	3.732	3.517	2.151	1.834
	$(2\theta)^o$	23.87	25.302	41.950	49.670
T_s = 623K	d_{hkl}	-	3.513	-	-
t = 2000Å	$(2\theta)^o$	-	25.376	-	-
T_s = 573K	d_{hkl}	3.731	3.516	2.154	1.836
t = 2000Å	$(2\theta)^o$	23.826	25.308	41.904	49.605
T_s =523K	d_{hkl}	-	3.504	2.149	1.834
t = 2000Å	$(2\theta)^o$	-	25.393	42.004	49.669
Ts = 473K	d_{hkl}	-	3.510	2.149	1.831
t = 2000Å	$(2\theta)^o$	-	25.349	42.001	49.757
T_s = 473K	d_{hkl}	-	3.525	2.153	1.835
t = 2230Å	$(2\theta)^o$	-	25.358	42.061	49.795
T_s = 473K	d_{hkl}	-	3.527	2.151	1.838
t =1750Å	$(2\theta)^o$	-	25.226	41.959	49.533
T_s = 473K	d_{hkl}	-	3.524	2.149	1.839
t =1530Å	$(2\theta)^o$	-	25.249	41.995	49.499

The experimental values of, 2θ, and the corresponding values of, d spacing, of the CdSe thin films having different, t, and, T_s, along with the values of their bulk counterpart and JCPDS standards are presented in the Table 3.2. It is clearly observed from the table that all the diffraction spectra display the characteristic diffraction peaks of the hexagonal phase of CdSe. No other peak with measurable intensity from either CdSe or the constituents was obtained in the X-ray diffractogram taken on the

grown thin films. Hence it was confirmed that the CdSe thin films prepared and used in this study are of hexagonal ZnS type of crystal structure.

In this case, it is seen that [002] plane is very clear and dominant, however, a small percentage of the orientations of [110], [112] and [100] planes also appear in these films depending upon the T_s of deposition. Dominance of the [002] hexagonal reflection indicates that the preferential growth of crystallites is in this particular direction, with c axis perpendicular to the surface of the substrate. All the XRDs presented here are of annealed CdSe thin films. The increase in the sharpness of the peaks in case of annealed films than that of 'as-deposited' films indicates the increase of crystallinity due to recrystallization effect.

Different structural parameters of CdSe thin films, of same, t, but deposited at different T_s and of films of different, t, but deposited at same T_s, are calculated by using the relevant formulae and are systematically represented in Table 3.3. The data of the table show variations in the structural parameters with, T_s & t and also with crystallographic orientations. The calculated values of lattice parameters are found to be in agreement to the already reported values /50,51/. The corrected values of lattice constants, estimated from the Nelson-Riley plots shown in Figs 3.7(a to j), are found to be in the range of 4.286 to 4.304Å for, a, and 6.992 to 7.020Å for, c. The values of lattice parameters, a, and, c, micro strain, ε, and grain size, D, are correlated with both T_s and, t, and are depicted in Figs 3.8(a to d) & Figs 3.9(a to d) respectively. The correlation with T_s shows that with increase of T_s the lattice constants, a, and, c, initially increase and reach a maximum at around 560K and then shows a decreasing trend. Variation of lattice constant is also observed with, t. There is a change in lattice constants for the deposited thin films over the bulk values, which suggest that film grains are strained. This may be due to change of nature and concentration of the native defects. The density of the films is therefore expected to change in accordance with the change of lattice constant /52/.

As observed from Fig 3.8(a), the grain sizes corresponding to [002] hexagonal reflection of the films increases with T_s. For the same plane the grain sizes are found to increase with, t, also, as shown in Fig 3.9(c), for the film grown at T_s = 473K. It is to be noted that the variation in grain size within the thickness range 1750 to 2230Å is

not very significant. With the increase of T_s the crystallinity of the films improves substantially. This consequently effects in decreasing some intergrain boundary discontinuities. Similar results in vacuum evaporated CdSe thin films are also reported by other workers /53-55/. With increasing T_s, generally the peak intensity also increases and the peaks become sharper indicating larger crystallite size at elevated T_s. At higher T_s in the formation process of the films, ad-atoms possess greater mobility along direction parallel to the substrate surface which thus contributes to improvement of the crystallization processes.

The variation of strain with, T_s and, t, of films are shown in Fig. 3.8(d) and Fig 3.9(d) respectively. The standard values of, a, and, c, for strain free bulk CdSe sample are 4.299Å & 7.010Å respectively /49/. Thus it is seen that observed values of, a, and c, are slightly greater for films deposited at T_s = 523K and 573K than their bulk counterparts whereas the values nearly coincide for film deposited at 623K and t = 2000Å. The observed values of, a, and, c, are less than the lattice parameters of the bulk CdSe for films deposited at T_s = 473K and thickness 2000Å. This is also true for the other films deposited at T_s = 473K within the thickness range 1530 to 2230Å, as observed from Table 3.3. This indicates that the grown films are under compressive strain /56, 57/. Fig 3.10(a) and Fig 3.10(b) show the variation of strain with grain size for the most preferred plane for two sets of CdSe thin film samples. It is clear from the plots that there is a decrease in the strain with the increase of grain size for films of different t as well as T_s.

Fig 3.11(a) and Fig 3.11(b) show the variation of dislocation density of CdSe thin films with T_s and t, for films of constant t and constant T_s respectively. It is observed that dislocation density decreases with t and T_s. But the decrease in dislocation density with film thickness is not very significant. It is therefore confirmed that in thin films containing smaller grain size the number of dislocation density is more. As a result of annealing also the number of dislocation density near grain boundary is reduced. The variation of dislocation density of CdSe thin films with strain, for films of constant t and constant T_s respectively are shown in Fig 3.12(a) and Fig 3.12(b). It is clear from the figures that dislocation density has a linear relation with strain.

Table 3.3 Calculated values of structural parameters of CdSe thin films, of constant t = 2000Å, deposited at different, T_s and of CdSe thin films, of different, t, deposited at constant T_s = 473K

t(Å) and T_s(K) of thin films	[hkl] values of planes	Lattice constant a(Å)	a(Å) from N-R plots	Lattice constant c(Å)	c(Å) from N-R plots	Grain sizes D(Å)	ε in 10^{-3}	δ in 10^{11} cm^{-2}
623K 2000Å	002	4.2989	-	7.0115	-	350	4.70	0.81
573K 2000Å	100	4.3072	4.3045	7.0250	7.0205	268	6.52	1.39
	002	4.3102		7.0299		308	5.35	1.05
	110	4.3066		7.0241		295	3.42	1.14
	112	4.3062		7.0234		253	3.40	1.56
523K 2000Å	002	4.2960	4.3020	7.0067	7.0175	283	5.80	1.24
	110	4.2968		7.0081		301	3.34	1.10
	112	4.3011		7.0150		201	4.26	2.47
473K 2000Å	002	4.3033	4.2865	7.0187	6.9921	280	5.90	1.27
	110	4.2971		7.0086		253	3.97	1.56
	112	4.2939		7.0033		221	4.17	2.04
473K 2230Å	002	4.3010	4.2811	7.0163	6.9810	323	5.10	0.95
	110	4.2913		6.9991		341	2.95	0.85
	112	4.2906		6.9979		326	2.63	0.94
473K 1750Å	002	4.3239	4.2930	7.0524	7.0055	275	6.20	1.32
	110	4.3012		7.0153		185	5.46	2.92
	112	4.3120		7.0329		145	5.95	4.75
473K 1530Å	002	4.3201	4.2950	7.0461	7.0075	171	9.67	3.41
	110	4.2977		7.0096		167	6.01	3.58
	112	4.3140		7.0374		228	3.78	1.92

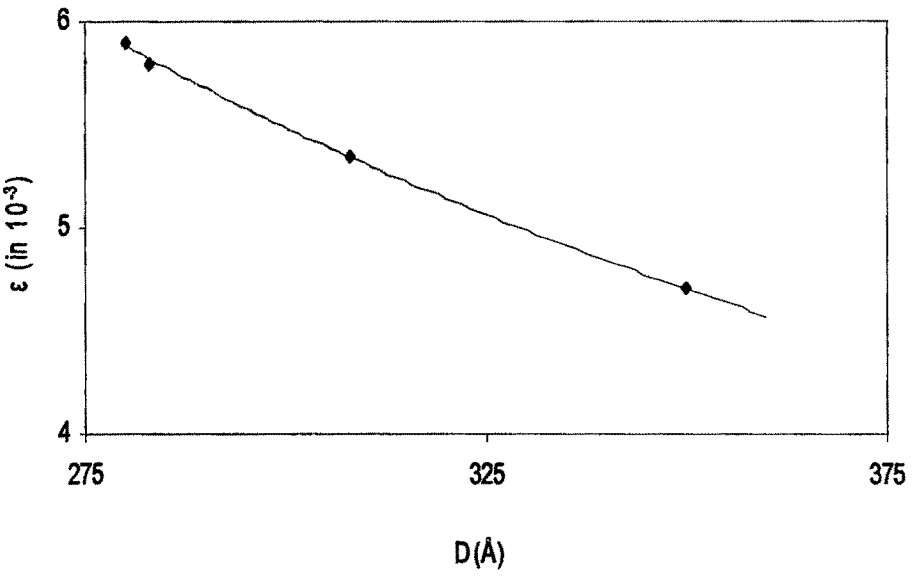

Figure 3.10(a) Variation of strain with grain size (D) of CdSe thin films of t = 2000Å and grown at different T_s

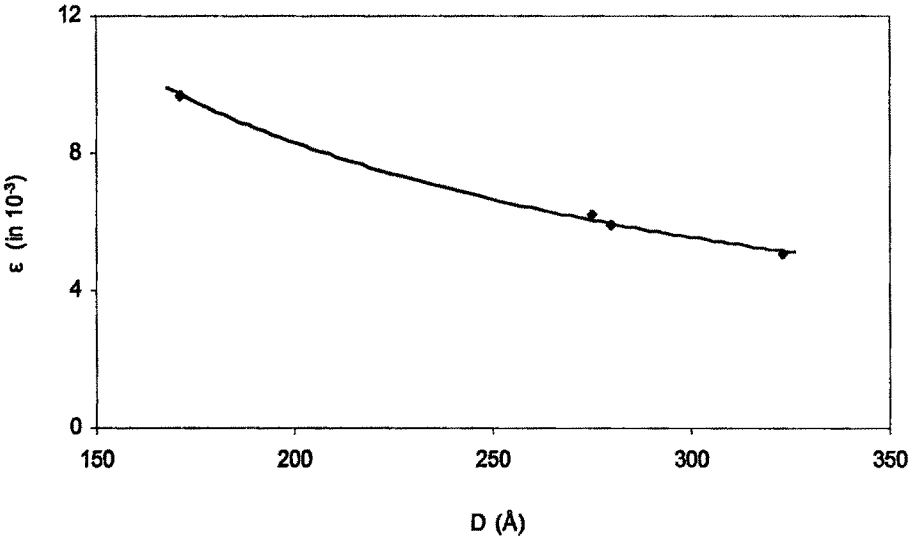

Figure 3.10(b) Variation of strain with grain size (D) of CdSe thin films of different, t and deposited at T_s = 473K

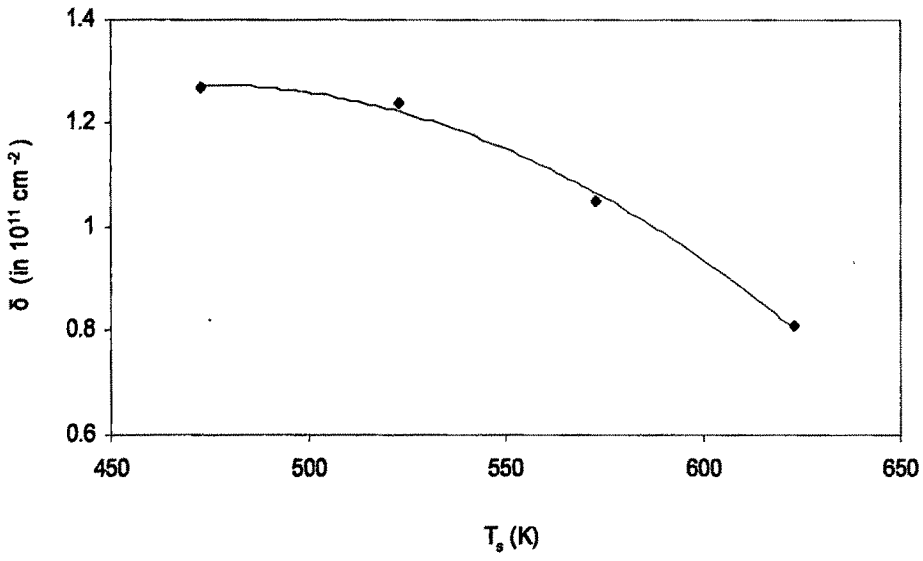

Figure 3.11(a) Variation of dislocation density with T_s(K) of CdSe thin films of constant t = 2000Å.

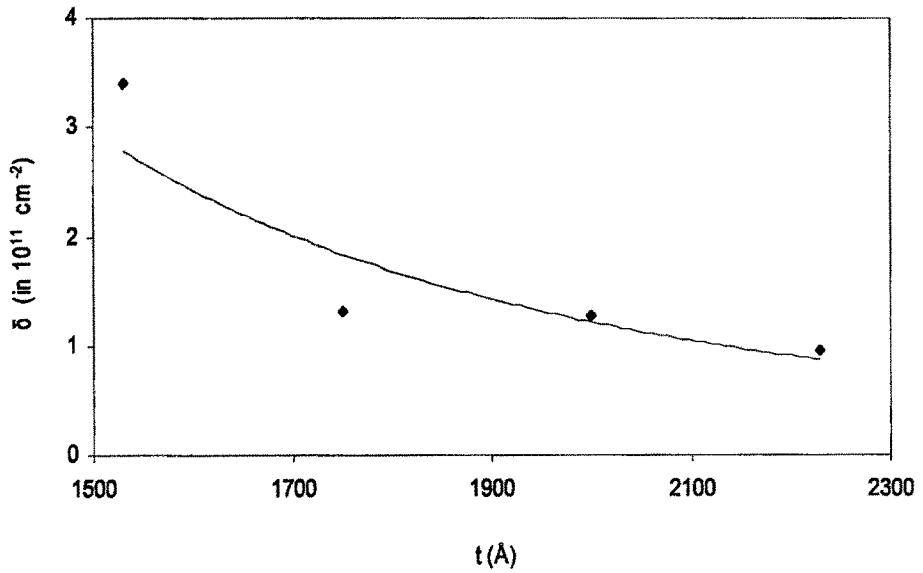

Figure 3.11(b) Variation of dislocation density with t(Å) of CdSe thin films grown at T_s = 473K

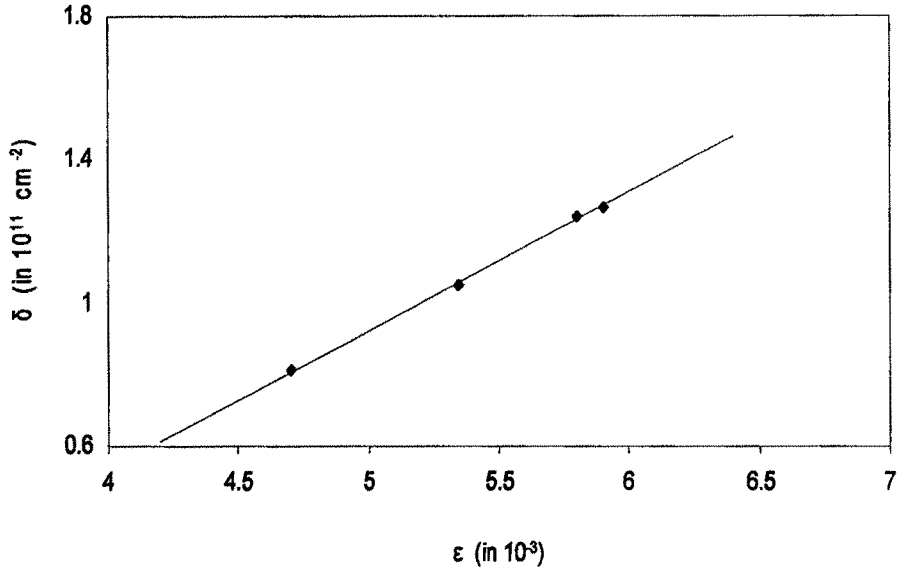

Figure 3.12(a) Variation of dislocation density with strain of CdSe thin films of constant t = 2000Å grown at different T_s.

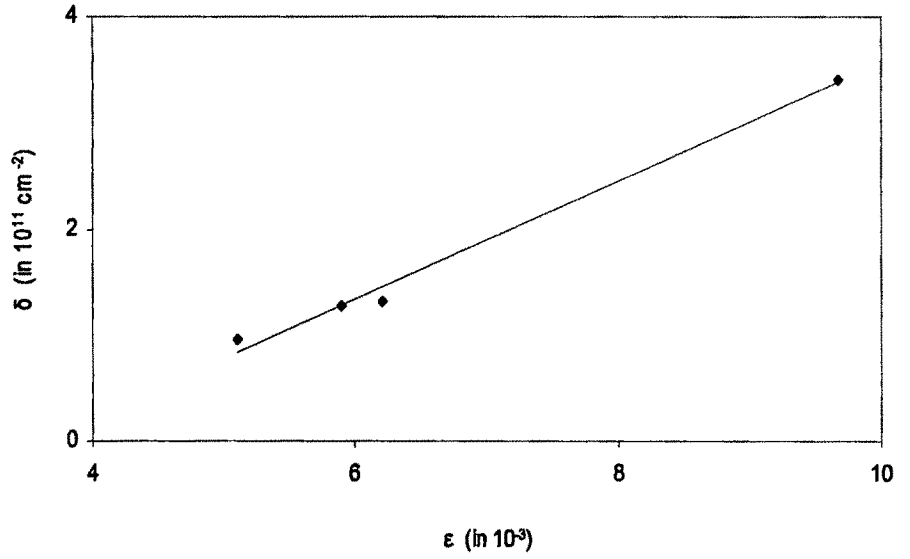

Figure 3.12(b) Variation of dislocation density with strain of CdSe thin films of different thickness grown at T_s = 473K.

3.5 Morphological study of CdSe thin films

3.5.1 SEM analysis

Scanning electron microscopy (SEM) is a convenient technique to study the microstructure of thin films /57/. Surface morphological study of the thermally deposited CdSe thin films were carried out by using the Scanning Electron Microscope operated with an accelerating voltage of 18kV. Figs 3.13(a to d) show the scanning electron micrographs of a CdSe thin film of thickness 2000Å deposited at T_s = 473K taken at different magnifications. In SEM observations of thin films, in case of higher magnifications, the inner and smaller particles are observed whereas in case of low magnifications the particles of larger size are observed. The film morphology under such studies shows that the films deposited at higher T_s are fairly uniform, homogeneous, polycrystalline and there are no macroscopic defects like peeling or cracks. Thus it is clear from the micrographs that the quality of the CdSe thin films, thermally deposited at elevated temperatures, is quite suitable for photoconductivity studies with good reproducibility. The crystallite sizes revealed from the SEM pictures are found to be higher than the average crystallite size values calculated from that of XRD analysis. The difference is probably due to calculated average grain size value and the value of individual grain size. The scanning electron micrograph of the CdSe film indicate that the film has a little rough surface which may be suitable for solar cell applications as it will capture more light /58,59/.

3.5.2 EDAX analysis

The quantitative analysis of CdSe films were carried out by using EDAX (Energy Dispersive Analysis of X-ray) technique for 'as-deposited' CdSe thin films grown on glass substrates, at different points to study the stochiometry of the films. Fig 3.14 shows a typical EDAX pattern and details of relative analysis for a CdSe thin film. The elemental analysis was carried out only for Cd and Se; the average atomic percentage of Cd:Se was 50.87:49.13, showing that the sample was slightly Se deficient. The Si peak that is observed in the EDAX pattern is due to the glass substrates used for deposition of CdSe thin films.

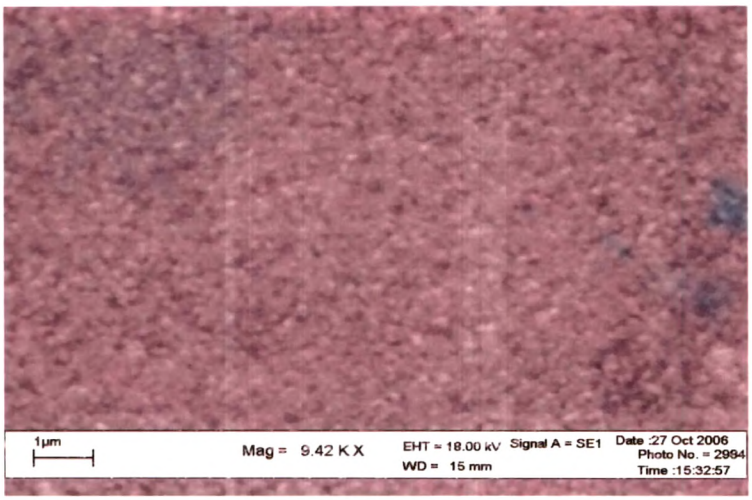

Figure 3.13(a) SEM photograph of a CdSe thin film of t = 2000Å deposited at T_s = 473K (Magnification 9.42kX)

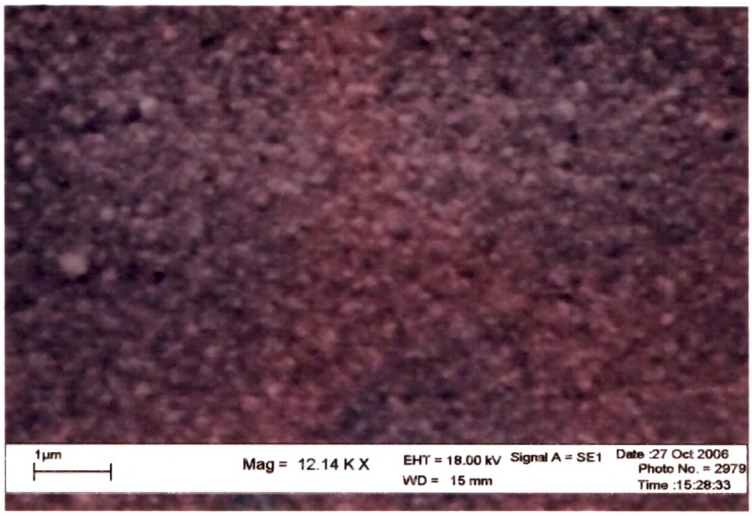

Figure 3.13(b) SEM photograph of a CdSe thin film of t = 2000Å deposited at T_s = 473K (Magnification 12.14kX)

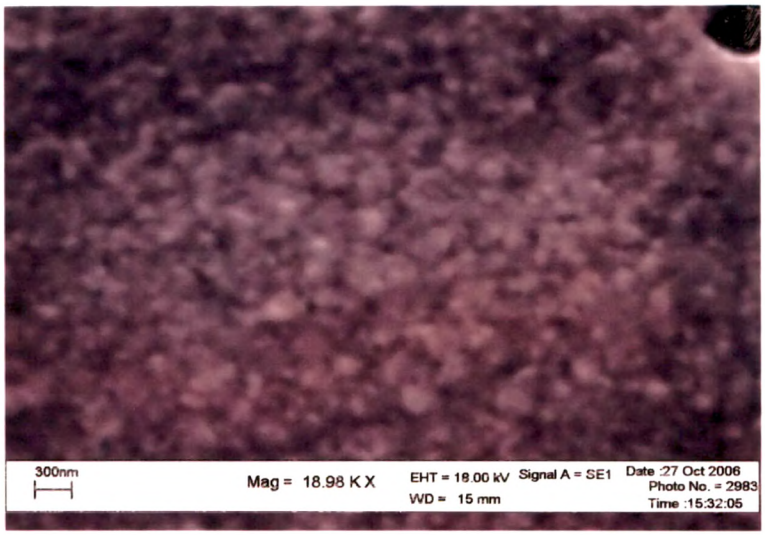

Figure 3.13(c) SEM photograph of a CdSe thin film of t = 2000Å deposited at T_s = 473K (Magnification 18.98kX)

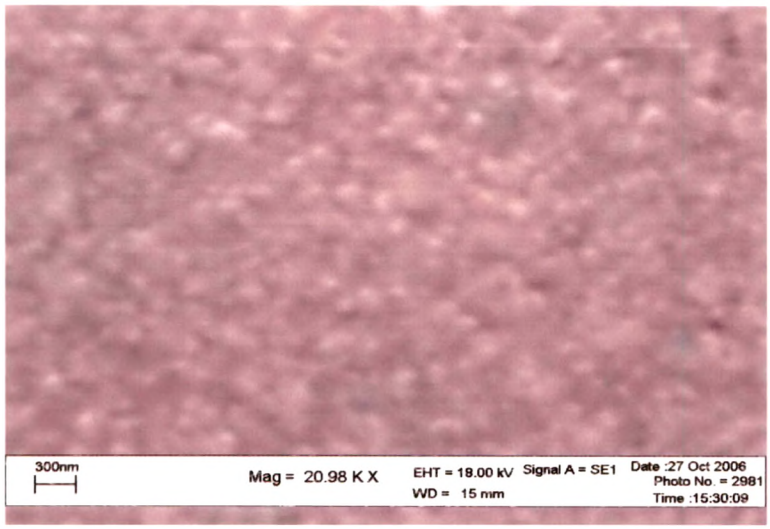

Figure 3.13(d) SEM photograph of a CdSe thin film of t = 2000Å deposited at T_s = 473K (Magnification 20.98kX)

ELEMENT	WEIGHT%	ATOMIC%
Se L	40.42	49.13
Cd L	59.58	50.87
TOTAL	100.00	100.00

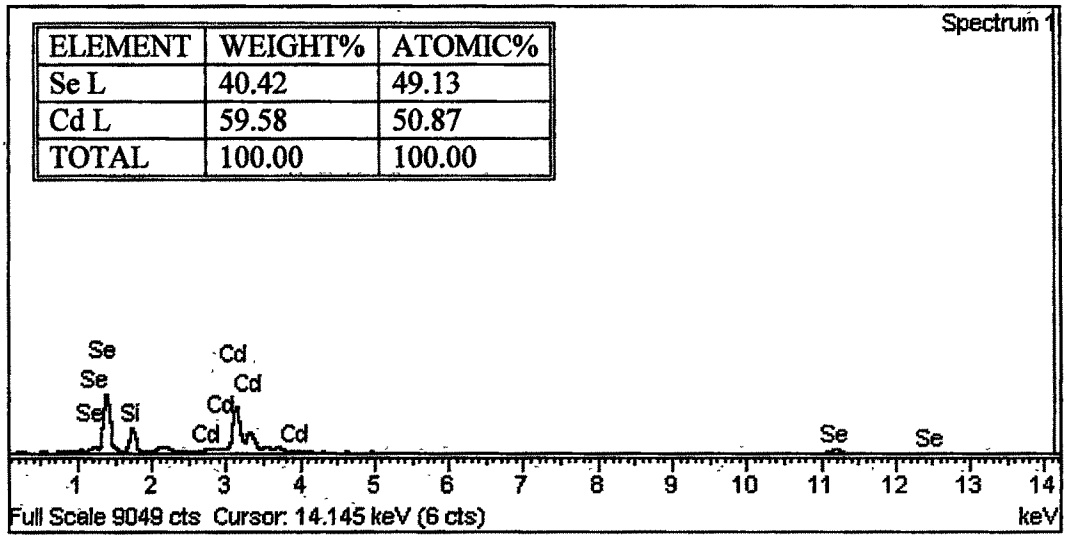

Figure 3.14 Typical EDAX pattern along with relative analysis of an 'as-deposited' CdSe thin film of t = 2000Å deposited at elevated T_s = 473K

3.5.3 XRF analysis

For elemental analysis of grown CdSe films, the films were loaded into a Perspex mask of WDXRF spectrometer. The X-ray tube was operated at 40kV and 40mA. The characteristics of the X-rays originated from the sample were analyzed by LiF 200, LiF 220 and PX1 crystal using Flow and Scintillation tandem detectors. Software program was made using X40 software and recorded the scanning of CdSe thin films. Figs 3.15(a to d) show the XRF spectra of an 'as-deposited' CdSe thin film grown at T_s = 300K. The spectrum in Fig 3.15(a) shows two peaks of SeK_β and $SeK_{\alpha 1}$ lines, which indicates the presence of Se in the sample film, along with two unknown peaks. The spectrum in Fig 3.15(b) shows, single peak of $CdK_{\alpha 1}$ lines along with $SbK_{\alpha 1}$ lines. Fig 3.15(c) shows the presence of $ZrK_{\alpha 1}$ and SeK_β lines where as Fig 3.15(d) shows the peak of SeL_α lines along with MgK_α and NaK_α lines. Peaks for Zr, Mg and Na appear from the target and probable impurities present in glass substrate used. The unknown peaks were not identified as the supporting peaks were not found. The presence of such peaks at the same positions for analyzed samples, other than CdSe, indicated that these were not related with CdSe sample. The qualitative analysis of thermally deposited CdSe films by XRF spectrometer confirms the presence of Cd and Se elements without incorporation of any impurities.

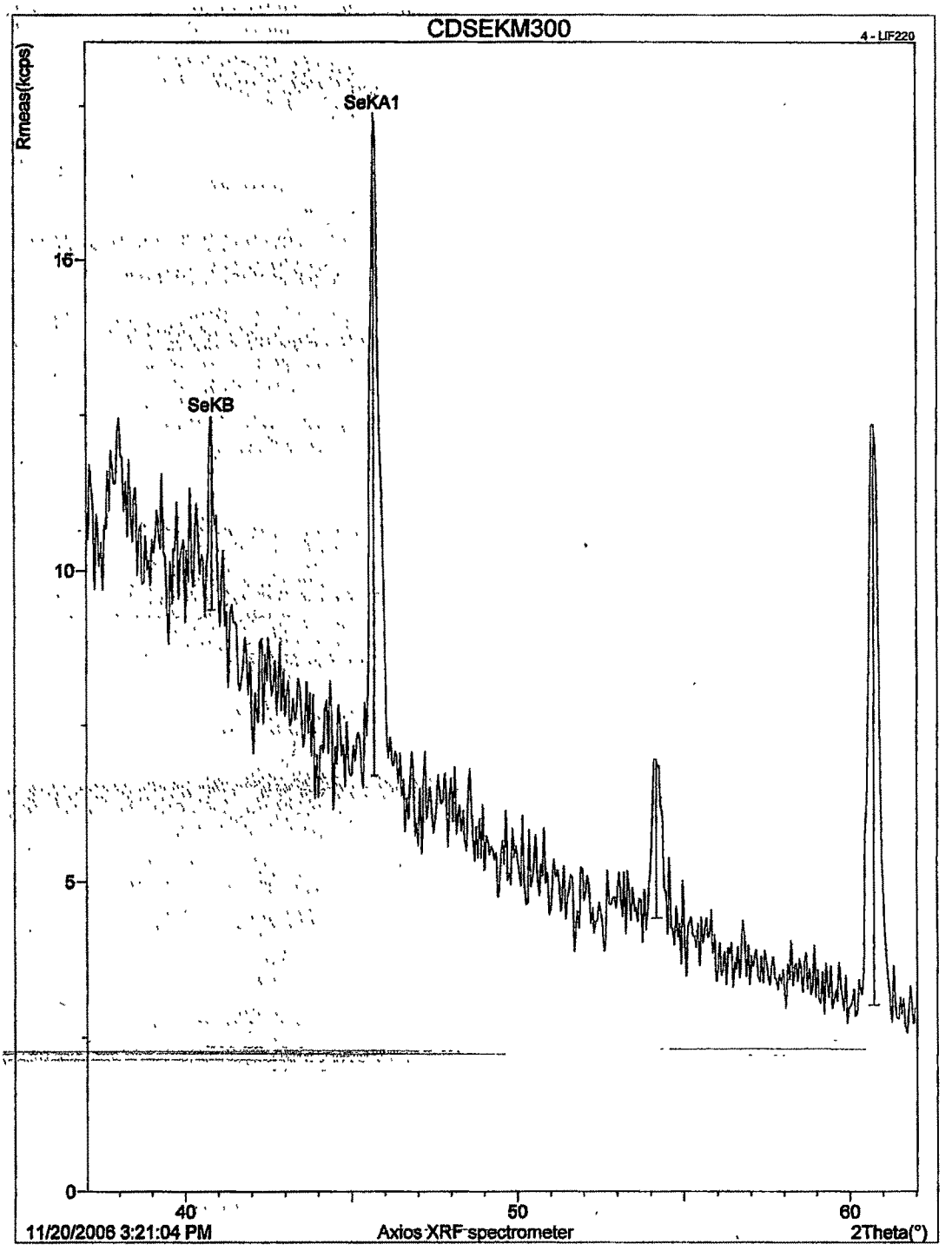

Figure 3.15(a) XRF spectra of an 'as-deposited' CdSe thin film showing SeK_{β} and $SeK_{\alpha 1}$ lines along with two unknown peaks (T_s = 300K)

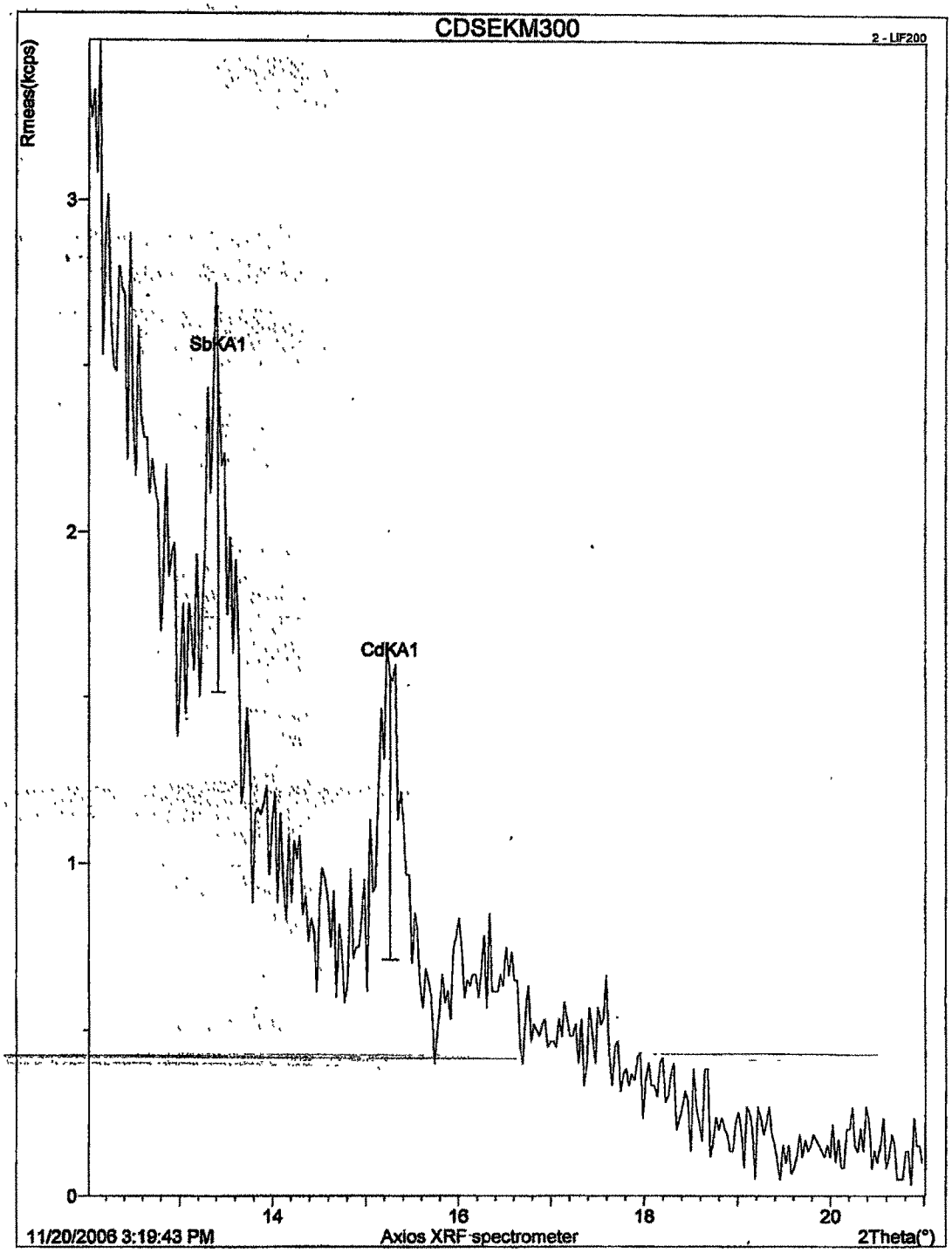

Figure 3.15(b) XRF spectra of an 'as-deposited' CdSe thin film showing peaks for $SbK_{\alpha 1}$ and $CdK_{\alpha 1}$ lines (T_s = 300K).

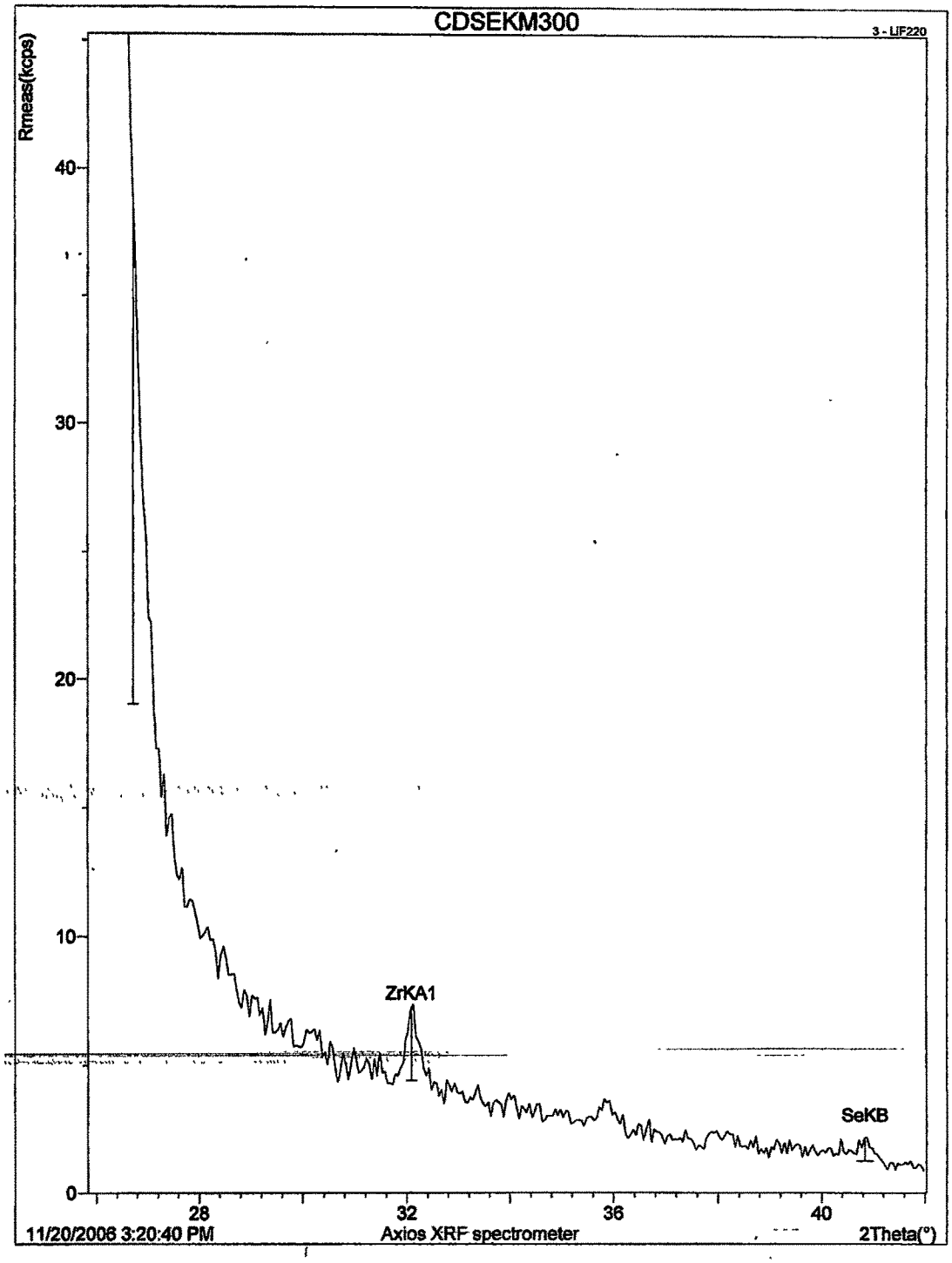

Figure 3.15(c) XRF spectra of an 'as-deposited' CdSe thin film showing $ZrK_{\alpha 1}$ and SeK_{β} lines (T_s = 300K).

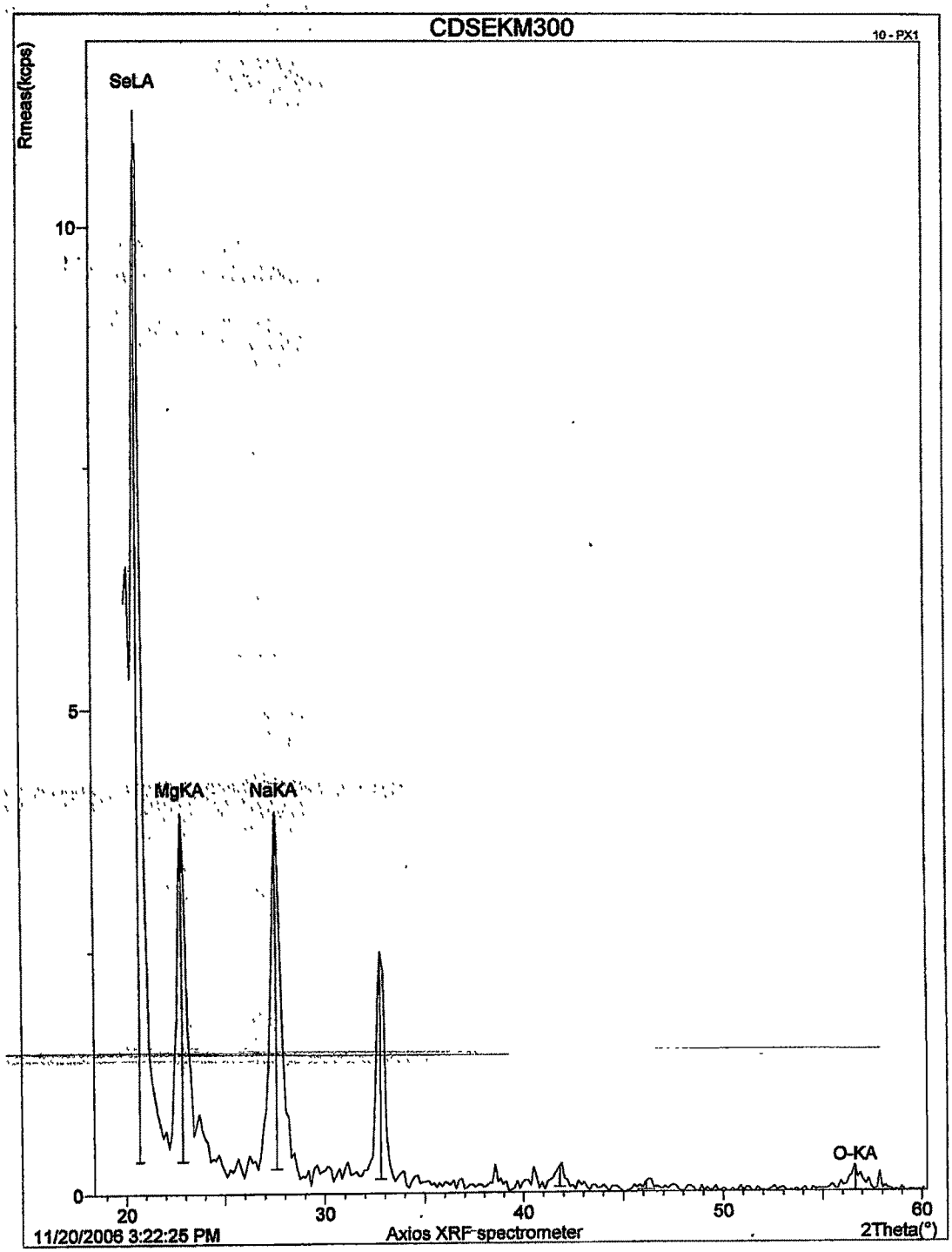

Figure 3.15(d) XRF spectra of an 'as-deposited' CdSe thin film showing SeL_{α}, MgK_{α} & NaK_{α} lines along with a small O-K_{α} and an unknown peak (T_s =300K).

3.6 Conclusions

As observed from the XRD analysis CdSe powder used as the source material to prepare the thin films are of hexagonal phase. The CdSe films thermally deposited at room temperature are amorphous and those grown at higher T_s range 473 to 623K and thickness range 1530 to 2230Å are polycrystalline in nature having hexagonal ZnS type structure. The most preferred orientations for CdSe thin film is along the hexagonal [002] direction. Orientations along [110], [112] and [100] directions are relatively in smaller percentage.

Certain changes have been observed in structural parameters such as lattice constant, grain size, average strain and dislocation density with both T_s of deposition and the thickness of the films. For constant thickness the grain size of the films for the most preferred orientation increases with the increase of T_s, this tells about the improvement of the crystallinity of the films. The grain size also increases with the thickness of the films for constant T_s. This signifies that there is an increase in the polycrystalline nature of the films with increase of film thickness. There are also observable changes in the structural parameters along different orientations. This means that variation in the structural configuration of the films is there from orientation to orientation. At any deposition temperature variation in lattice constants of the deposited thin films over the bulk, suggests that built-in strains are present in the film grains and for these films built-in microstrains are dependent of the temperature of deposition.

Scanning Electron Microscope observations show the polycrystalline growth for the films deposited at higher T_s and such films are suitable for the photoconductivity studies as has been observed in the subsequent chapters. The results of XRF spectra and EDAX analysis shows that 'as-deposited' CdSe thin films are free from impurity, contains Cd and Se elements in nearly in equal proportion. This indicates that the grown CdSe thin films are acceptably stochiometric.

3.7 References

1. Y. Zhang, B. J. Skromme and F. S. Turco-Sandroff; *Phys. Rev. B*, 46(7),1992, 3872

2. J. H. Chang, M. W. Cho, H. M. Wang, H. Wenisch, T. Hanada, T. Tao, K. Sato and

O. Oda; *Appl. Phys. Letts.*, 77(9), 2000, 1256-1258.

3. D. Samanta, S. Ghoral, B.K. Samantary, A. K. Chaudhari and U. Pal; *Indian J. of Pure and Appl. Phys.*, 32, 1994, 910.
4. U.Pal, R. Silva-Gonzalez, G. Martinez-Montes, M. Garacia-Jimeney, M.A. Videl, and Sh.Torres; *Thin Solid Films*, 305, 1997, 346.
5. J. Hamersky, *Thin Solid Films*. 381, 1976, 101
6. K. N. Shreekanthan, B. V. Rejendra, V. B. Kasturi and G. K. Shivakumar, *Cryst. Res. Technol.*, 38(1), 2003, 30-33.
7. S. Mader; in L. I. Maissel and R. Glang (Eds), *Hand Book of Thin Film Technology*, Mc Graw Hill, N. Y., 1970, Chap 9-1
8. R. E. Thun; in G. Hass (Eds), *Physics of Thin Films*, Vol 1, Academic Press, N. Y., 1963, 187.
9. H. P. Klug and L. E. Alexander; *X-ray Diffraction Procedures*, John Wiley & Sons, Inc, N. Y., 1954.
10. K. L. Chopra; *Thin Film Phenomena*, Robert E Krieger Publishing Company, Huntington, N.Y., 1969, 110.
11 A. Banerjee; in K. L. Chopra and L. K. Malhotra (Eds), *Thin Film Technology and Applications*, Tata-McGraw- Hill, New Delhi, 1985, 71.
12. A. Goswami; *Thin Film Fundamentals*; New Age International (P) Limited, Publishers, New Delhi, 1996, Chap. 2.
13. T. Fuji, M. Yamaguchi and M. Suzuki; *Rev. Sci. Instrum.*, 66(3), 1995, 2504
14. M. Shiojiri and E. Suito; *Jpn. Jour. Appl. Phys.*, 3(6), 1964, 314.
15. S. Saha, U. Pal, B. K. Samantaray, A. K. Chaudhury and H. D. Banerjee; *Thin Solid Films*, 164, 1988, 85.
16. G. S. R. Rao and S. J. Reddy, *Thin Solid Films*, 120, 1984, 205.
17. L. Dapkus, K. Valacka, J. Bakutis and V. Jasutis, *Sov. Phys. Collect* (USA) 21(1), 1981, 39.
18. A. L. Dawar, C. Jagadish, K. V. Ferdinand, A. Kumar and P. C. Mathur. *Applications of Surface Science*; 23, 1985, 846.
19. Y. Yasuda, *Jap. J. Appl. Phys.*; 7(10), 9, 1985, 1171.
20. H. Okimura and Y. Sakai, *Jap. J. Appl. Phys.*; 7(7), 1988, 731.

21. S. M. Petal and N. G. Petal, *Thin Solid Films*, 122, 1984, 297.

22. P. K. Kalita, B. K. Sarma and H. L. Das; *Bull. Mat. Sci.*, 23(4), 2000, 313.

23. C. K. De and N. K. Misra; *Ind. Jour. Phys.*, 71A(5), 1997, 339.

24. C. K. De, N. K. Misra and T. B. Ghosh; *Ind. Jour. Phys.*, 69A(2), 1995, 264.

25. N. Junqua and J. Grithe, *Thin Solid Films*, 250, 1994, 37.

26. H. Ijichi, O. Tadanaga, A. Otsuka, M. Murakami, *Thin Solid Films*, 250,1994, 165

27. M. A. Kenawy, H. A. Zayed, A. M. Ibrahim and A. El-Shazly, *Indian J. Pure and Appl. Phys.*; 9, 1991, 625.

28. M. Azoulay, E. Grossman, H. Schacham, M. Mizrachi, A. Raizman; *J. Mater. Sci.*, 30, 1995, 4527.

29. R. Venugopal, R. P. Vijayalaskshmi, D. R. Reddy, B. K. Reddy; *J. Mater. Sci.*; 31,1996, 4082.

30. B. E. Warren, *X-ray Diffraction*, Addison Wesley Publishing Co., London, 1969, 81 .

31. A. Goswami, *Fundamentals of Thin Films*, New Age International (P) Ltd., New Delhi, 1996, 106.

32. K. Zanio, *Semi conductor and Semi metals*; 13, Cadmium Telluride, Academic Press, N.Y., 1978, 54.

33. M. J. Tafreshi, K. Balakrishnan, R. Dhanaselearan; *J. Mater. Sc.*, 32, 1997, 3518

34. A. H. Sid, S. Mahmoud, *J. Mater. Sci. Letters*, 11,1992, 938.

35. H. P. Klug and L. E. Alexander; *X-ray Diffraction Procedures*, John Wiley & Sons, Inc, N.Y., 1954, Chap 3, 151.

36. I. H. Khan in *Hand Book of Thin Film Technology* (Eds) L. I. Maissel and R. Glang, Mc-Grow Hill Co., N.Y.,1970, Chap. 9, 19.

37. N. F. N. Henry, H. Lipson and W. A. Wooster, *The Interpretation of X-ray Diffraction Photographs*, Mc. Millan and Co. Ltd., 1961, 179-80.

38. B. D. Cullity; *Elements of X-ray Diffraction* (2nd Edition), Addision-Wesley Publishing Company, Inc, London,1978, Chap 10, 327-335.

39. W. L. Roth; in M. Aven and J. S. Prener (Eds) *Physics and Chemistry of II-VI Compounds*, North-Holland Publishing Co., Amsterdam, 1967,124.

40. G. A. Jeffrey, G. S. Parry and R. L. Mozzi, *J. Chem. Phys.*, 25(5), 1956, 1024

41. H. P. Klug and L. E. Alexander, *X-ray Diffraction Procedures*, John Wiley & Sons, Inc. N. Y., 1954, Chap 9, 512.

42. S. Sen, S. K. Halder and S. P. Sen Gupta; *J. Phys. Soc.*, Japan, 38(6), 1975, 1643-1645.

43. M. Bedir, M. Oztas, O. F. Bakkaloglu ,R. Ormanci, *Eur. Phys. J. B.* 45, 2005, 465

44. D. Venkatachalam, D. Mangalaraj, Sa. K. Narayandass, K. Kim and J. Yi, *Phys B*, 358, 2005, 27

45. D. P. Padiyan, A. Marikani and K. R. Murali, *Mat. Chem. and Phys.* 78, 2002, 51

46. S. Lalitha, R. Sathyamoorthy, S. Senthilarasu, A. Subbarayan and K. Natarajan, *Solar En. Mat. & Solar Cells*; 82, 2004, 187-199.

47. A. R. Verma, O. N. Srivastana, *Crystallography Applied to Solid State Physics* (2nd Ed) Wiley Eastern Ltd., 1991, 356.

48. J. B. Nelson and D. P. Riley ; *Proc. Phys. Soc.* (London) 57, 1945, 160.

49. Powder Diffraction Data File, *Joint Committee of Powder Diffraction Standard*, International Center for Diffraction Data, USA (1984), Card No. 8-459, p 143.

50. N. G. Dhere, N. R. Parikh and A. Ferreir, *Thin Solid Films*; 44, 1977, 83.

51. I. B. Rufus, V. Ramakrishnan, B. Viswanathan, J. C. Kuriacse, *J. of Mater. Sci. Lett.*, 11, 1992, 252.

52. P. K. Kalita, B. K. Sarma and H. L. Das; *Bull. Mater. Sci.* 26(6), 2003, 613.

53. K. R. Murali, K. Srinivasan and D. C. Trivedi, *Materials Letters*, 59, 2005, 15-18.

54. K. R. Murali, K. Srinivasan and D. C. Trivedi, *Mater. Sc. & Eng. B*, 111, 2004, 1.

55. H. P. Sarma, V. Subramaniam, N. Rangarajan and K. R. Murali, *Bull. Mater. Sci*, 18, (7),1995, 879.

56. P. J. Sebastian, *Thin Solid Films*; 221,1992, 233.

57. R. B. Kale, S. D. Sartale, B. K. Chougule and C. D. Lokhande, *Semicond. Sci. Technol.* 19, 2004, 980.

58. B. Bozzini, C. Lenardi and N. Lovergine, *Materials of Chemistry and Physics*, 66(2-3), 2000, 219.

59. B. Maiti, P. Gupta, S. Choudhary and A. K. Pal, *Thin Solid Films*, 1984-85, 104.

****